



City Research Online

City, University of London Institutional Repository

Citation: Zhou, S-Q., Yang, Y-F. & Fu, F. (2023). Performance of SSC filled circular steel tube short columns under axial compression. *Structures*, 57, 105147. doi: 10.1016/j.istruc.2023.105147

This is the accepted version of the paper.

This version of the publication may differ from the final published version.

Permanent repository link: <https://openaccess.city.ac.uk/id/eprint/31532/>

Link to published version: <https://doi.org/10.1016/j.istruc.2023.105147>

Copyright: City Research Online aims to make research outputs of City, University of London available to a wider audience. Copyright and Moral Rights remain with the author(s) and/or copyright holders. URLs from City Research Online may be freely distributed and linked to.

Reuse: Copies of full items can be used for personal research or study, educational, or not-for-profit purposes without prior permission or charge. Provided that the authors, title and full bibliographic details are credited, a hyperlink and/or URL is given for the original metadata page and the content is not changed in any way.

City Research Online:

<http://openaccess.city.ac.uk/>

publications@city.ac.uk

Performance of SSC filled circular steel tube short columns under axial compression

Shi-Qi Zhou^a, You-Fu Yang^{a,*}, Feng Fu^b

^a *State Key Laboratory of Coastal and Offshore Engineering, Dalian University of Technology, Dalian, 116024, China*

^b *Department of Engineering, School of Science & Technology, City, University of London, Northampton Square, London, UK, EC1V 0HB*

Abstract: Steel slag concrete (SSC) filled steel tube (SSC-FST), reusing the waste steel slag, is a new type of composite members, therefore shows advantages in sustainable use of resources. In order to investigate axial compressive performance of this new types of SSC-FST short columns with circular section, ten specimens with varied steel slag aggregate (SSA) replacement ratio and cross-sectional steel ratio (α) were tested. The failure patterns, load versus deformation relationship and mechanical indexes (axial capacity, elastic modulus and ductility) of the specimens were recorded and analyzed. The test results indicate that, generally, replacing natural aggregates with SSAs and improving α lead to better structural performance of circular SSC-FST short column specimens. Moreover, a refined finite element (FE) model considering the initial strain of core concrete before loading was established to simulate the performance of circular SSC-FST short columns under axial compression, and the FE model was validated through experimental results from this research and the literature. Based on the verified FE model, the mechanism of axially compressed circular SSC-FST short columns was further analyzed. Finally, simplified equations were proposed to predict the axial capacity of circular SSC-FST short columns, and generally the calculated results show good agreement with the numerical/experimental results.

Keywords: Steel slag concrete (SSC) filled steel tube; Circular section; Short columns; Axial compression; Finite element (FE) simulation; Simplified equations.

*Corresponding author. Tel.: 86-411-8470 8510; Fax: 86-411-8467 4141.

E-mail address: youfuyang@163.com (Dr. You-Fu Yang).

Nomenclature

A_c	cross-sectional area of core concrete	p	interaction stress
A_s	cross-sectional area of steel tube	R_c	coarse SSA replacement ratio
A_{sc}	cross-sectional area of composite column	R_f	fine SSA replacement ratio
C_n	axial capacity factor	SG	strain gauge
CS_{nc}	a kind of compressive strength of NC	$S_{M,p,c,max}$	maximum value of the maximum principal stress of core concrete
CS_{ssc}	a kind of compressive strength of SSC	$S_{M,s,max}$	maximum value of the Mises stress of steel tube
D	outer diameter	SSA	steel slag aggregate
DI	ductility index	SSC	steel slag concrete
DT	displacement transducer	SSC-FST	steel slag concrete filled steel tube
E_c	elastic modulus of concrete	t	wall thickness of steel tube
E_s	elastic modulus of steel	T	number of days from the end of the initial curing
$E_{sc}(E_{sc,c})$	composite elastic modulus	U_3	top displacement
f_{cu}	cubic compressive strength of concrete	α	cross-sectional steel ratio
FE	finite element	β_ε	reduction factor
f_{scy}	axial compressive capacity factor	ε	strain
f'_{ssc}	cylindrical compressive strength of SSC	ε_a	axial strain
f_{ssck}	characteristics compressive strength of SSC	$\varepsilon_{a,0.4}$	average axial strain when axial load equals to $0.4N_{ue}$
f_y	yield strength of steel tube	$\varepsilon_{a,y}$	axial strain while reaching f_{scy}
IS	initial strain of plain concrete	$\varepsilon_{c(s)}$	strain of concrete (steel)
L	height of column	ε_h	hoop strain
N	axial load	ε_i	initial strain of core concrete before loading
NA	natural aggregate	$(\varepsilon_{sh})_T$	shrinkage strain of concrete
NC	normal concrete	$\varepsilon_{sh,u}$	ultimate shrinkage strain
NCA	natural coarse aggregate	$\sigma_{c(s)}$	stress of concrete (steel)
NFA	natural fine aggregate	σ_{sc}	axial stress over composite section ($=N/A_{sc}$)
N_u	axial capacity	σ_{ue}	nominal ultimate strength ($=N_{ue}/A_{sc}$)
N_{uc}	simplified axial capacity	ξ_s	confinement factor
N_{ue}	tested axial capacity	Δ	axial shortening
$N_{u,fe}$	simulated axial capacity		

1. Introduction

Steel slag, from the reaction of flux and iron ore, is an industrial by-product of steel manufacture, which has the characteristics of good activity, rich content of free calcium and magnesium oxides, high content of heavy metals, and so on [1]. In China, the steel production reached 1.04 billion tons in 2021, resulting in approximately 150 million tons of steel slag. Although the government has

1 promoted the reuse of steel slag, only about 22% steel slag is reused [2]. Currently, a large amount of
2 steel slag has been accumulated for long time, and thus a large area of land has been occupied, causing
3 huge waste of resource and serious environmental pollution.
4

5 Simultaneously, due to higher strength and better angularity of steel slag than natural sand and
6 gravel, as well as the presence of certain hydraulic cementitious properties, the steel slag can serve
7 as a cementitious material [3], aggregates [4-8], or mineral admixture [9] for new concrete after
8 treatment. In general, owing to better angularity of steel slag aggregate (SSA), the bond performance
9 between the aggregate particles and the cement paste is increased, leading to higher values of
10 compressive, tensile and flexural strength of steel slag concrete (SSC) [10-12]. The SSC may also
11 have good microstructure and interface between aggregates, which enhances its impermeability [13].
12 However, the free CaO and free MgO composition in the steel slag lead to volume expansion of new
13 concrete and thus threaten the safety of structures, which limits the utilization of the SSC [14, 15].
14
15

16 It is well known that, due to the interaction and coordination between outer steel tube and its core
17 concrete, concrete filled steel tube (CFST) structural form is usually characterized by high strength,
18 good plasticity and ductility, and excellent fire-resistant and seismic performance, and has been
19 widely used in civil engineering structures [16]. Moreover, in terms of economic benefits, outer steel
20 tube in the CFST can also serve as the forms for casting concrete, thus accelerating the construction
21 progress and saving the materials. Shrinkage of core concrete in the CFST members, however, has a
22 negative impact on their structural behaviour, and replacing natural aggregate (NA) with SSA is one
23 effective solution to reduce the shrinkage of core concrete considering the expansion characteristics
24 of the latter [17]. Filling the SSC into the steel tube, named as steel slag concrete filled steel tube
25 (SSC-FST), can increase the bond between steel tube and its core concrete due to the expansion
26 performance of the SSC [5, 17, 18], and thereby can make the SSC have a good application prospect.
27 This also helps to solve the serious environmental pollution caused by the large accumulation of steel
28 slag and protect the precious natural resources.
29
30

31 At present, the research towards structural behaviour of the SSC-FST members is generally in its
32
33
34
35
36
37
38
39
40
41
42
43
44
45
46
47
48
49
50
51
52
53
54
55
56
57
58
59
60
61
62
63
64
65

1 early phase, and the available experimental studies include axial compressive performance of short
2 columns [17-20], flexural properties of beams [19], interfacial bond properties [5] and hysteretic
3 performance of beam-columns [21]. It is further discovered that, with respect to the axially
4 compressed circular SSC-FST short columns, current limited experimental results [17, 18, 20]
5 showed that the failure pattern of the specimens with SSC was similar to that of the reference
6 specimens with normal concrete (NC); however, the structural performance of the former was
7 generally better than the latter. Moreover, Yu et al. [18] and Lai et al. [20] also carried out a numerical
8 modelling of circular SSC-FST short columns subjected to axial compression, and generally good
9 conformity between the simulated and measured results was obtained. Nevertheless, the initial
10 deformation characteristics of core concrete before loading and the contribution of the SSA presence,
11 which have obvious influence on the mechanical property of core SSC, were not considered in their
12 numerical models.
13
14
15
16
17
18
19
20
21
22
23
24
25
26

27 The above analysis shows that more experiments on the axially compressed circular SSC-FST short
28 columns need to be carried out, and it is necessary to further develop a numerical simulation model
29 considering the initial strain of core SSC before loading, so as to fully understand the performance
30 and mechanism while subjected to concentric compression, and eventually obtain the axial capacity
31 prediction model. The aim of this study is thus to comprehensively understand the structural
32 behaviour of circular SSC-FST short columns under axial compression. The test results of ten
33 specimens with SSA replacement ratio and cross-sectional steel ratio as parameters are first presented.
34 A refined finite element (FE) model considering the initial strain of core SSC before loading is then
35 established to model the axial compressive performance of circular SSC-FST short columns, and the
36 FE model is verified by comparing simulation results to experimental results. In addition, the effects
37 of initial strain of core SSC and other main parameters on the performance and representative
38 mechanism of axially compressed circular SSC-FST short columns are analyzed using the FE model.
39 The reasonable simplified equations are also proposed for axial capacity prediction of circular SSC-
40 FST short columns.
41
42
43
44
45
46
47
48
49
50
51
52
53
54
55
56
57
58
59
60
61
62
63
64
65

2. Experimental investigations

2.1. Specimen preparation

A total of 10 composite specimens with circular section, including 8 SSC-FST short columns and 2 conventional CFST short columns as reference, were fabricated, and all specimens had a same height (L) of 450 mm and a same outer diameter (D) of 150 mm. The key parameters varied in the tests included: (1) coarse SSA replacement ratio (R_c): 0, 50% and 100%; (2) fine SSA replacement ratio (R_f): 0, and 50%, and (3) cross-sectional steel ratio (α): 0.094 and 0.135. In this study, R_c and R_f are defined as the ratio of the mass of coarse SSA or fine SSA to that of all coarse or fine aggregate, respectively, and α is defined as cross-sectional area of steel tube (A_s) divided by cross-sectional area of core concrete (A_c).

Table 1 summarizes the information of the specimens, in which t is the wall thickness of steel tube; f_y is the yield strength of steel tube; f_{cu} is the cubic compressive strength of concrete for compression tests of composite short columns; N_{ue} is the tested axial capacity; $N_{u,fe}$ is the simulated axial capacity; and E_{sc} is the composite elastic modulus. In Table 1, 'C1' and 'C2' in the specimen labels donate α of 0.094 and 0.135, respectively, and the second and the third part of the specimen labels represent the numerator of R_c and R_f , respectively.

Rolling operation was employed to fabricate all the circular steel tubes, and there was one straight butt weld on each tube. The welding quality was strictly controlled to guarantee effective transfer of the loads. Before casting the concrete, one square steel plate with 210 mm side length and 15 mm thickness was welded to the end of steel tube as the bottom endplate. After 14 days of curing, the concrete surface was first grinded to be flush with the top surface of steel tube to make sure that both can take the axial compressive loads together, and then another square steel plate same as the bottom endplate was welded to the top surface of steel tube. In addition, eight pairs of right-angle trapezoidal stiffeners with 10 mm thickness spaced equally along the circumference were welded simultaneously to the outer wall of steel tube and the endplate to avoid the unexpected end destruction during loading process.

2.2. Material properties

1 Axial tensile tests were carried out on three standard coupons. The obtained average yield strength
2
3 (f_y), modulus of elasticity (E_s), ultimate strength and Poisson's ratio for circular steel tubes with
4
5 $t=3.33$ mm were 449.7 MPa, 1.89×10^5 N/mm², 526.9 MPa and 0.264, respectively; whereas the
6
7 corresponding values for circular steel tubes with $t=4.59$ mm were 518.5 MPa, 1.87×10^5 N/mm²,
8
9 611.9 MPa and 0.253, respectively.
10

11
12
13 The steel slag concrete (SSC) in this study was prepared by replacing some or all of the natural
14
15 aggregate (NA) with the screened steel slag aggregate (SSA) produced by a basic oxygen furnace,
16
17 and both coarse SSA and fine SSA were settled for two years. The gradation of natural coarse
18
19 aggregate (NCA), i.e. limestone, ranged from 5 mm to 31.5 mm, and the coarse SSA had a same
20
21 particle grading range as the NCA. The gradation of natural fine aggregate (NFA), namely yellow
22
23 sand, ranged from 0.16 mm to 5 mm, and the fine SSA also possessed a same gradation as the NFA.
24
25 The chemical compositions of steel slag were same as those in [19]. Table 2 provides the apparent
26
27 gravity, bulk density, absorption rate, crushing index and fineness modulus of different aggregates.
28
29 Other materials were: P.O 42.5 cement, fly ash, tap water and polycarboxylate superplasticizer.
30
31
32
33
34

35 Five types of concrete were prepared, and the mix proportions and properties of concrete are
36
37 described in Table 3, where E_c is the modulus of elasticity, $f_{cu,28}$ is the 28-day cubic compressive
38
39 strength, and IS is the initial strain at the beginning of axial compression tests on composite
40
41 specimens and the minus values represent the shrinkage strain. The cubic compressive strength was
42
43 obtained by axial compression tests on concrete cubes of 150 mm×150 mm×150 mm, and the
44
45 modulus of elasticity was obtained through axial compression tests on concrete prisms of 150
46
47 mm×150 mm×300 mm. The shrinkage strain was measured by concrete prisms of 100 mm×100
48
49 mm×300 mm. The results showed that, after replacing NAs with SSAs, the slump of fresh concrete
50
51 reduced, due to higher absorption rate, more angular steel slag particles and larger frictional resistance
52
53 of SSAs than those of NAs. It can also be found from Table 3 that, the SSC has a larger $f_{cu,28}$, f_{cu}
54
55 and E_c than the reference NC, and the addition of fine SSA has a more significant impact on the
56
57
58
59
60
61
62
63
64
65

improvement of cubic compressive strength. This may be due to the fact that, compared with NAs, the surface of SSA particles is rougher, which allows a stronger bond with the cement paste, and the smaller the particle size of SSAs, the larger the contacting area with the hydration products. Similar experimental phenomena were also found in [4, 10, 15]. Additionally, the *IS* of the SSC is smaller than that of the NC, due to the presence of free CaO and free MgO having expansive properties in the steel slag, and the fine SSA plays a more significant role in reducing the shrinkage strain of new concrete [17].

2.3. Tests under axial compression

A 5000 kN capacity testing machine was chosen to carry out the tests of composite short specimens under axial compression. The test set-up is illustrated in Fig. 1. The specimen was vertically placed on the lower platen, and a load cell was arranged between the top endplate of the specimen and the upper platen to detect the evolution of axial compressive loads. To monitor axial shortening, four displacement transducers (DTs) symmetrically placed on the lower platen were prepared. To detect the strain development at the mid-height section, the strain gauges (SGs) were placed at four measuring points evenly distributed around the circumference (90 degrees apart), and each measuring point was set with an axial SG and a hoop SG.

A loading scheme of load control followed by displacement control [22] was utilized in the tests. Before the axial compressive load reached 90% of the simulated peak load using the FE model introduced later, the tests were continuously proceeded based on the loading rate, which was set to be 0.5 kN/s. After that, the tests was controlled by a displacement rate of 0.1 mm/min until the termination of the tests.

2.4. Test results and discussion

For all the specimens, the failure process generally consisted of three phases, that is, elastic, elastic-plastic, and post-peak. At the initial loading phase, the axial load increased almost linearly with the increase of axial shortening, and the appearance of the specimens remained intact basically. When the load reached approximately 75% of the ultimate load, the growth rate of axial load was gradually

1 lower than that of axial shortening, and the diagonal shear-slip lines begun to appear on outer wall of
2 steel tube accompanied by the noise of concrete crushing/cracking. When approaching ultimate load,
3
4 the number of the diagonal shear-slip lines on the outer wall of steel tube gradually increased, and
5
6 there was a slight bulging of steel tube at both ends of the shear-slip lines. After the ultimate load was
7
8 attained, with the increase of axial shortening, the axial load decreased rapidly at first and the
9
10 decreasing rate reduced gradually until the end of the tests, and simultaneously the shear-slip
11
12 deformation together with local bulging of steel tube and the crushing/cracking of concrete further
13
14 progressed. It should be noted that the bonding between SSC and steel tube might be critical for the
15
16 axial and lateral compression behaviour of the composite columns [23], which needs further
17
18 investigation.
19
20
21
22
23

24 The failure pattern of the specimens is shown in Fig. 2(a), in which dashed lines indicate the shear-
25
26 slip band on steel tube, and arrows point to local bulging of steel tube. The pictures demonstrate that,
27
28 for the specimens with the same α , the difference in core concrete type (i.e. R_c and/or R_f) has
29
30 limited influence on the failure pattern of the specimens. Moreover, with the growth of α , i.e. from
31
32 0.094 (C1 series specimens) to 0.135 (C2 series specimens), the dip angle of the shear-slip band on
33
34 the steel tube decreases and the local bulging of steel tube becomes slighter. This can be explained
35
36 that, in the case of having similar material properties, a larger α means a better confinement of steel
37
38 tube to its core concrete, which makes the specimen show a steadier failure characteristic.
39
40 Additionally, in the area corresponding to the shear-slip band on the steel tube, there is also an
41
42 diagonal zone including both crushing and cracking of concrete, and the destruction of core concrete
43
44 is generally the most serious in the region where the local bulging occurs to the steel tube, as
45
46 demonstrated in Fig. 3(a).
47
48
49
50
51
52

53 Fig. 4 indicates the measured axial load (N) versus axial shortening (Δ) curves of the specimens.
54
55 It is shown that, in general, there are three sequential phases in all $N - \Delta$ curves, namely, the first
56
57 approximative elastic phase in which N increases with the increase of Δ at an almost fixed slope,
58
59 the second elastic-plastic phase in which N improves with the growth of Δ at a gradually decreased
60
61
62
63
64
65

slope until achieving ultimate load, and the third post-peak phase in which N decreases with the rise of Δ at a gradually decreased slope. Under the same α , the SSA replacement ratio (R_c and/or R_f) has a moderate impact on the trend of $N - \Delta$ curves. However, when core concrete is the same, the $N - \Delta$ curve of the specimens with a larger α generally has a greater initial slope, a longer elastic-plastic phase and a slower load decline rate at the post-peak phase, owing to the increased confinement of steel tube to its core concrete. The axial capacity (N_{ue}) of composite specimens is determined to be the ultimate load on the $N - \Delta$ curve, as presented in Table 1.

The axial load (N) versus strain (ε) curves of the specimens are displayed in Figs. 5 (a-1) and (b-1), where both axial and hoop strains are taken as the average of the measured values of four strain gauges. As can be seen in the figures, the evolution of the $N - \varepsilon$ curves is generally similar to that of the $N - \Delta$ curves. Moreover, the change of R_c and/or R_f mainly affects the post-peak part of the $N - \varepsilon$ curves, but there is no consistent change in the decline trend, and a larger α generally result in a larger axial/hoop strain of the specimens while reaching N_{ue} .

Fig. 6 demonstrates the relationship between N/N_{ue} and $|\varepsilon_h/\varepsilon_a|$ of the specimens, where ε_a and ε_h are the average value of the recorded axial and hoop strains, respectively. It can be found that, the $N/N_{ue} - |\varepsilon_h/\varepsilon_a|$ relationship generally exhibits similar characteristics as the $N - \Delta(\varepsilon)$ curves. Before the N/N_{ue} value reaches about 0.75 (i.e. in the approximative elastic phase), the $|\varepsilon_h/\varepsilon_a|$ values are generally close to the Poisson's ratio of steel. When the N/N_{ue} value is between 0.75 and 1.0 (i.e. in the elastic-plastic phase), the $|\varepsilon_h/\varepsilon_a|$ values exceed the Poisson's ratio of steel and gradually increase. In addition, when $\alpha=0.094$, the $|\varepsilon_h/\varepsilon_a|$ values of the specimens containing different types of concrete differ greatly, and circular SSC-FST specimens have larger $|\varepsilon_h/\varepsilon_a|$ values than their reference counterpart; however, when $\alpha=0.135$, the difference in the $|\varepsilon_h/\varepsilon_a|$ values of the specimens containing different types of concrete becomes smaller, and circular SSC-FST specimens have smaller $|\varepsilon_h/\varepsilon_a|$ values than their reference counterpart. This is mainly due to the fact that, a larger α means a better confinement from steel tube to its core concrete, leading to a more stable transverse deformation of core concrete, and some unpredictable defects in the tests cause

the inconsistency of the relative difference in the $N/N_{ue} - |\varepsilon_h/\varepsilon_a|$ relationship between the specimens with SSC and the reference specimens with NC. In the post-peak phase, the trend of the $N/N_{ue} - |\varepsilon_h/\varepsilon_a|$ relationship is significantly determined by the soundness of SGs and the difference between the position of SGs and that of the shear-slip band on the steel tube.

To quantitatively measure the difference between axial capacity of circular SSC-FST specimens and that of their reference counterparts (i.e. circular CFST specimens), the axial capacity factor (C_n) is defined as follows:

$$C_n = \frac{N_{ue,ssc}}{N_{ue,nc}} \quad (1)$$

where, the subscripts 'ssc' and 'nc' denote composite specimens with SSC and the reference NC, respectively.

Fig. 7 illustrates the effect of parameters on N_{ue} and C_n of the specimens. It is shown that, overall, all circular SSC-FST specimens have a higher N_{ue} than their reference counterparts, and a larger α leads to a higher N_{ue} for the specimens containing the same concrete. The circular SSC-FST specimen with $R_c=50\%$, $R_c=100\%$, $R_f=50\%$ and $R_c=R_f=50\%$ respectively results in a C_n of 0.998, 1.038, 1.016 and 1.243 when $\alpha=0.094$, and C_n respectively equals to 1.060, 1.050, 1.145 and 1.192 when $\alpha=0.135$. These data show that, generally, the axial capacity of circular SSC-FST specimens is improved more obviously than that of their reference counterparts when both R_c and R_f are 50% or $\alpha=0.135$ and replacing NFA with fine SSA is more effective to increase the axial capacity of circular SSC-FST short columns when SSA replacement ratio is the same. These can be explained that, the SSC has a high compressive strength than the reference NC, especially when the core concrete contains fine SSA, and a larger α means that steel tube possesses a better constraint to its core concrete.

Referring to the way for conventional circular CFST [24], the composite elastic modulus (E_{sc}) of circular SSC-FST short column specimens is defined to evaluate the ability of resisting axial shortening, and the detailed formula is as follows:

$$E_{sc} = \frac{0.4\sigma_{ue}}{\varepsilon_{a,0.4}} \quad (2)$$

where, σ_{ue} ($=N_{ue}/A_{sc}$) is the nominal ultimate strength, A_{sc} is the cross-sectional area of composite column, and $\varepsilon_{a,0.4}$ is the average axial strain when axial load equals to $0.4N_{ue}$. The obtained results of E_{sc} are listed in Table 1.

As mentioned above, the recorded N - ε_a curve of the specimen is generally in the elastic stage when the load is less than $0.75N_{ue}$. Therefore, based on the superposition principle, the composite elastic modulus of the specimens ($E_{sc,c}$) can also be calculated using the following formula:

$$E_{sc,c} = \frac{E_c + \alpha \cdot E_s}{1 + \alpha} \quad (3)$$

The variation of E_{sc} and $E_{sc}/E_{sc,c}$ of the specimens is displayed in Fig. 8. It is shown that, generally, circular SSC-FST specimens have a higher E_{sc} than their reference counterparts, and the specimens having a larger α result in a higher E_{sc} when core concrete keeps the same. On average, E_{sc} of circular SSC-FST specimens is 6.9% higher than that of their reference counterparts, and the specimens with α of 0.135 have a 14.5% higher E_{sc} than those with α of 0.094. Moreover, the values of $E_{sc}/E_{sc,c}$ vary between 0.852 and 0.998, with a mean value of 0.931 and a standard deviation of 0.050, showing that the composite elastic modulus of circular SSC-FST short columns generally can be acquired by the superposition principle.

Taking the method in [24] as reference, the definition of ductility index (DI) of composite specimens is as follows:

$$DI = \frac{\Delta_{-85\%}}{\Delta_{ue}} \quad (4)$$

where, $\Delta_{-85\%}$ is the axial shortening corresponding to $85\%N_{ue}$ in the post-peak phase, and Δ_{ue} is the axial shortening while reaching N_{ue} .

Fig. 9 exhibits the ductility index (DI) of the specimens. It can be seen that, when α increases the ductility of the specimens improves, owing to the fact that thicker steel tube can better constrain the damaged core concrete in the post-peak phase. Moreover, the specimens containing SSC generally

have a smaller DI than the corresponding specimen with NC, which may be caused by the existence of empty micro-pores in the SSC [4].

3. Numerical simulation

3.1. Description of the FE model

A refined finite element (FE) model was established to simulate the axially compressed circular SSC-FST short columns using the software package ABAQUS [25], which was widely used in the numerical simulation of CFST members. As given in Table 3, the shrinkage occurs to all the five types of concrete before applying axial compression to the composite specimens, and to account for this in the FE model, the entire simulating process was divided into two successive analysis stages. In stage 1, the field variables of core concrete were first obtained by including the deformation characteristics of concrete before loading in the FE model, and then the numerical results of core concrete were imported into stage 2 as the initial conditions. In stage 2, the axial compressive performance of composite short columns was simulated.

Before the SSC is stressed, the shrinkage strain is generated when the expansion deformation caused by free oxides in the SSA is smaller than the shrinkage deformation of all components; otherwise, the expansion strain is generated, which mainly depends on the type, content and treatment of SSAs. For example, the four types of SSC in this study are produced using coarse SSA and/or fine SSA aged for 2 years and the IS is the shrinkage strain (see Table 3), while the IS can be either shrinkage strain or expansion strain in the tests of Yu et al. [17] through completely replacing the sand using fine SSA. It should be noted that, generally, only shrinkage strain is generated for the NC. As is concluded [26], the shrinkage of core concrete in the CFST is smaller than that of plain concrete, i.e., the measured IS of plain concrete cannot be directly used in the FE modelling of axially compressed circular SSC-FST short columns, and it is necessary to convert IS into the corresponding initial deformation of core concrete before loading.

The investigation outcomes [26] show that, generally, the shrinkage strain of plain concrete and core concrete in the CFST can be accurately predicted by the formula in ACI 209 [27]:

$$(\varepsilon_{sh})_T = \frac{T}{35+T} \cdot \varepsilon_{sh,u} \quad (5)$$

where, $(\varepsilon_{sh})_T$ is the shrinkage strain of concrete; T is the number of days from the end of the initial curing; and $\varepsilon_{sh,u}$ is the ultimate shrinkage strain equal to $780\gamma_{sh} \times 10^{-6}$, and γ_{sh} is the product of multiple correction factors.

To address the gap in shrinkage strain between plain concrete and core concrete in the CFST [26], a reduction factor (β_ε) is defined:

$$\beta_\varepsilon = \frac{(\varepsilon_{sh})_{T,cfst}}{(\varepsilon_{sh})_{T,pc}} \quad (6)$$

where, the subscripts 'cfst' and 'pc' represent core concrete in the CFST and plain concrete, respectively.

According to ACI 209 [27], β_ε is mainly related to the sizes (e.g. volume-surface ratio) and the ambient relative humidity under identical curing time and mix proportion, that is, loading age, fine aggregate percentage, cement content and air content are the same. In this study, the real sizes of two kinds of concrete are used, and the ambient relative humidity of plain concrete and core concrete in the CFST is respectively taken as 70% and 90% based on actual curing conditions [26].

After obtaining β_ε , the initial shrinkage strain (ε_i) of core concrete in the SSC-FST and the CFST before being stressed can be determined using the following formula:

$$\varepsilon_i = \beta_\varepsilon \cdot IS \quad (7)$$

The calculated ε_i of the specimens is also listed in Table 3.

Moreover, as there was no report related to the discrepancy in the expansion characteristics between core concrete in the CFST and plain concrete, the initial expansion strain (ε_i) of core concrete in the SSC-FST and the CFST is temporarily set to be the IS of plain concrete.

The circular steel tube was replicated using a classical metal plasticity model in ABAQUS [25]. The measured results of steel tube were directly taken as its properties in the elastic stage. The real stress versus plastic strain relationship requiring to be input the software was obtained by the

engineering stress (σ_s) versus strain (ε_s) relationship including five phases, which can better simulate the plastic property of circular steel tube [24, 28]:

$$\sigma_s = \begin{cases} E_s \cdot \varepsilon_s & (\varepsilon_s \leq \varepsilon_e) \\ -A \cdot \varepsilon_s^2 + B \cdot \varepsilon_s + C & (\varepsilon_e < \varepsilon_s \leq \varepsilon_{e1}) \\ f_y & (\varepsilon_{e1} < \varepsilon_s \leq \varepsilon_{e2}) \\ f_y \cdot \left(1 + 0.6 \frac{\varepsilon_s - \varepsilon_{e2}}{\varepsilon_{e3} - \varepsilon_{e2}}\right) & (\varepsilon_{e2} < \varepsilon_s \leq \varepsilon_{e3}) \\ 1.6f_y & (\varepsilon_s > \varepsilon_{e3}) \end{cases} \quad (8)$$

where, $\varepsilon_e = 0.8\varepsilon_y$, $\varepsilon_{e1} = 1.2\varepsilon_y$, $\varepsilon_{e2} = 12\varepsilon_y$, $\varepsilon_{e3} = 120\varepsilon_y$, $A = 0.2f_y/(\varepsilon_{e1} - \varepsilon_e)^2$, $B = 2A \cdot \varepsilon_{e1}$, $C = 0.8f_y + A \cdot \varepsilon_e^2 - B \cdot \varepsilon_e$ and $\varepsilon_y = f_y/E_s$.

In order to well depict the structural property of core SSC, the damaged plasticity model [25] was chosen. In the elastic stage, the Poisson's ratio was taken as 0.2 [29], and E_c was set to be $4730\sqrt{f'_{SSC}}$ [30], in which f'_{SSC} is the cylindrical compressive strength. In the plastic stage, a constant value of 40° for dilation angle was adopted, and the other plasticity parameters used in the modelling were same as those in [19]. The equation suggested by Birtel and Mark [31] was used to determine the compressive damage factor of core SSC. Moreover, the stress-inelastic strain relationship of core SSC under compression needing to be input the software was obtained by the compressive stress (σ_c)-strain (ε_c) relationship in [19]:

$$\frac{\sigma_c}{f'_{SSC}} = \begin{cases} 2(\varepsilon_c/\varepsilon_{c,u}) - (\varepsilon_c/\varepsilon_{c,u})^2 & (\varepsilon_c/\varepsilon_{c,u} \leq 1) \\ \frac{\varepsilon_c/\varepsilon_{c,u}}{\beta_0 \cdot (\varepsilon_c/\varepsilon_{c,u} - 1)^2 + \varepsilon_c/\varepsilon_{c,u}} & (\varepsilon_c/\varepsilon_{c,u} > 1) \end{cases} \quad (9)$$

where, $\varepsilon_{c,u} = (1300 + 12.5f'_{SSC} + 800\xi_s^{0.2}) \times 10^{-6}$, $\xi_s = \alpha \cdot f_y/f_{SSCk}$, $\beta_0 = 1.25\sqrt{f'_{SSC}} \times (2.36 \times 10^{-5})^{[0.25 + (\xi_s - 0.5)^7]} \geq 0.12$, ξ_s is the confinement factors of SSC-FST [19], and f_{SSCk} is the characteristics compressive strength of SSC that equal to 67% of cubic compressive strength [24]. In this study, f'_{SSC} is converted from the cubic compressive strength based on the suggestion in EN 1992-1-1 [32].

In the absence of experiments on the compressive strength of SSC, the following formulae can be adopted for calculating all kinds of compressive strength of SSC [19]:

$$CS_{scc} = \begin{cases} (0.4R + 1.0) \cdot CS_{nc} & (R < 0.3) \\ (-0.15R + 1.165) \cdot CS_{nc} & (0.3 \leq R \leq 1.0) \end{cases} \quad (10)$$

where, CS_{scc} and CS_{nc} are a kind of compressive strength of SSC and that of the corresponding NC, respectively, and R is the SSA replacement ratio, for SSC with coarse SSA or fine SSA, R respectively equals to R_c or R_f , while for SSC with both coarse and fine SSA, R is equal to half the sum of R_c and R_f .

According to the achievement in [19], the tensile property of core SSC in the plastic stage was simulated using cracking criterion based on fracture energy, and the cracking stress was taken as $0.1f'_{ssc}$.

For the boundary conditions in stage 1, the ‘Tie’ constraint was defined as the contact between different components, considering that the stress of different components caused by the initial strain of core concrete is relatively small and cannot damage the interface between steel tube and core concrete. All degrees of freedom of lower surface of bottom endplate were restricted, i.e. being defined as the ‘ENCASTRE’, and all degrees of freedom of upper surface of top endplate were not restricted. At the same time, the initial shrinkage/expansion strain (ϵ_i) was applied by cooling/heating the core concrete part. For the boundary conditions in stage 2, the definition of constraint between steel tube and core concrete was transformed into the ‘hard contact’ in normal direction and the ‘Coulomb friction’ in tangential directions, and the constraint between endplates and core concrete was defined as the ‘hard contact’ in normal direction. For upper surface of top endplate, the restriction on translations in X and Y directions was employed. Before applying axial shortenings along Z direction (U_z) to the top endplate, the results obtained in stage 1 were introduced into the FE model in stage 2. The meshing together with boundary conditions of axially compressed circular SSC-FST short columns in the FE modelling are demonstrated in Fig. 10.

Fig. 11 shows the predicted field variables of specimen C1-50-50 before loading. It can be seen from Fig. 11(a) that, from the top to the bottom, the displacement along Z direction of steel tube and core SSC decreases from the maximum to zero; however, the displacement along the cross-section of steel tube is uniformly distributed, while that of core SSC is not uniformly distributed, considering

1 that the bond between outer tube and core SSC makes the thin steel tube (shell) does not form a
2 displacement gradient, whilst there is an evident displacement gradient for the solid core SSC. It is
3 indicated in Fig. 11(b) that, two kinds of stress are symmetric about the mid-height section. From
4 mid-height section to the junction of steel tube and stiffeners, two kinds of stress show a decreasing
5 trend, and there are also gradients of the maximum principal stress of core SSC, except for the core
6 concrete within the stiffener height range.
7
8
9
10
11

12 The effect of ε_i on typical field variables of all the specimens is demonstrated in Fig. 12, where
13 $S_{M,s,max}$ is the maximum value of the Mises stress of steel tube, $S_{Mp,c,max}$ is the maximum value of
14 the maximum principal stress of core concrete, and U_3 is the top displacement along the Z direction.
15 It is shown that, for the composite specimens with the shrinkage of core concrete, $S_{M,s,max}$, $S_{Mp,c,max}$
16 as well as U_3 increase with the increase of ε_i irrespective of concrete type, and the specimens with
17 a larger α possess a smaller $S_{M,s,max}$, $S_{Mp,c,max}$ and U_3 while ε_i keeps constant due to an
18 increased constraint of steel tube on its core concrete.
19
20
21
22
23
24
25
26
27
28
29
30

31 **3.2. Verification of the FE model**

32 The FE simulation results showed that the failure patterns of composite specimens with different
33 parameters were similar, and the differences between them were mainly lain in the detailed values of
34 the field variables after being compressed. The typical simulated failure pattern of whole specimen
35 and core concrete of axially compressed circular SSC-FST short columns and their reference
36 counterparts are demonstrated in Fig. 2(b) and Fig. 3(b), respectively. It can be found that, the
37 simulated outward bulging of steel tube and the dilation of core concrete are the most serious at the
38 mid-height section and weaken towards two ends constrained by the stiffeners, unlike the test results
39 in Figs. 2(a) and 3(a). Similar differences were also found in previous studies [33-35], mainly due to
40 the fact that, a few random defects in the materials and/or deviation in the tests could not be properly
41 included in the FE simulation. Overall, the predicted failure area and the maximum bulging
42 deformation of steel tube are consistent with the observations in the experiments.
43
44
45
46
47
48
49
50
51
52
53
54
55
56
57
58
59
60
61
62
63
64
65

The contrast between the simulated axial load (axial stress) versus axial shortening (axial strain) curves and the measured results from this research and the literature [17, 18, 20] is shown in Figs. 4, 5 and 13, where σ_{sc} ($=N/A_{sc}$) is the axial stress over composite section. As can be seen from the comparison that, the predicted $N - \Delta(\varepsilon_a)$ and $\sigma_{sc} - \varepsilon_a$ curves generally agree well with the measured ones; nevertheless, owing to the absence of the materials' defects and the experimental deviation in the FE model, there is a certain discrepancy between the simulated and measured curves, especially in the elastic-plastic and post-peak stage.

The FE simulated axial capacities ($N_{u,fe}$) of circular SSC-FST short columns are compared with the measured results in Fig. 14. The statistical results show that, the error between $N_{u,fe}$ and N_{ue} is generally less than 10%, and the mean value and standard deviation of $N_{u,fe}/N_{ue}$ are 0.963 and 0.051, respectively, showing that the axial capacity of circular SSC-FST short columns can be accurately predicted using the developed FE model, and the prediction is generally safe.

3.3. Mechanism analysis using the FE model

The impact of ε_i on the mechanism of circular SSC-FST short columns under axial compression was further studied by the validated FE model. The basic conditions included: $D=600$ mm, $L/D=3.0$, $\alpha=0.10$, $f_{cu}=60$ MPa, $f_y=355$ MPa, $R=50\%$, and $\varepsilon_i=-200\times 10^{-6}$, 0 and 200×10^{-6} . In the analysis, as can be seen from Fig.15, three representative points on the simulated $\sigma_{sc}-\varepsilon_a$ curves are chosen to illustrate the mechanism, where point A corresponds to the axial load of $0.4N_u$, point B corresponds to the axial load of N_u , point C corresponds to the axial strain of 0.02, and N_u is the axial capacity.

Fig. 16 demonstrates the stress field (S33) of core SSC at the mid-height section of typical circular SSC-FST short columns under different initial strain (ε_i). It can be seen that, as ε_i goes from negative (shrinkage strain) to positive (dilatation strain), the S33 tends to enhance, indicating that it is more favorable for the load carrying of composite columns when the core concrete initially expands (e.g. adding an expansion agent to the concrete). At point A, the distribution of S33 is almost uniform as core concrete bears axial loads independently. At point B, there is a stress gradient over cross-section, and the stress near the center is the smallest as the relatively small constraining effect of steel tube on

core concrete is transmitted from their contact surface to the central area. At point C, the stress gradient over cross-section is still obvious; however, the distribution property is opposite to that at point B, that is, the S33 reaches the maximum in the central region. This can be explained that, the large confinement effect of steel tube on core concrete makes concrete central zone more restrained.

The effect of initial strain (ε_i) and confinement factor (ξ_s) on the interaction stress (p) between steel tube and core concrete is presented in Fig. 17. It can be observed that, before being stressed, the initial dilation and shrinkage strain cause positive and negative p , respectively, and there is no interaction between steel tube and core concrete if the initial deformation characteristics of core concrete are not considered. At the initial phase, p has a process of first decreasing and then recovering to the initial value, considering that the Poisson's ratio of core concrete is smaller than that of steel tube, i.e., the transverse deformation of core concrete is less than that of steel tube. Subsequently, as loading continues, p increases continuously or increases and then decreases after reaching the maximum when the Poisson's ratio of core concrete exceeds the Poisson's ratio of steel tube, which mainly depends on the magnitude of ξ_s . Furthermore, with the increase of ε_a , the columns with different ε_i have a similar involvement of p , and the columns with a positive ε_i and a larger ξ_s result in a higher p due to the improved confinement of steel tube to its core concrete.

4. Simplified equations

Fig. 18 demonstrates the effect of typical parameters on $\sigma_{sc} - \varepsilon_a$ curve of circular SSC-FST short columns under axial compression. It is shown that, the cross-sectional steel ratio (α), the yield strength of steel tube (f_y), the cubic compressive strength of NC (f_{cu}), the initial strain (ε_i) and the SSA replacement ratio (R) have a significant impact on the $\sigma_{sc} - \varepsilon_a$ curve, while the diameter of steel tube (D) has a relatively small influence.

Referring to the previous achievements for circular CFST [24], the axial compressive capacity factor (f_{scy}) corresponding to a certain axial strain ($\varepsilon_{a,y}$) on the $\sigma_{sc} - \varepsilon_a$ curve of circular SSC-FST short columns is determined. The formula for $\varepsilon_{a,y}$ is as follows:

$$\varepsilon_{a,y} = [1300 + 12.5f'_{SSC} + (600 + 33.3f'_{SSC}) \cdot \xi_s^{0.2}] \times 10^{-6} \quad (11)$$

Through in-depth analysis of a large number of FE simulation results, it is found that, the influence of α , f_y , f_{cu} and R on f_{scy} of circular SSC-FST can be unified into the effect of ξ_s . The relationship between $f_{scy,0}/f_{ssck}$ and ξ_s is displayed in Fig. 19(a), where $f_{scy,0}$ is the axial compressive capacity factor without considering the initial strain of core concrete. Based on the regression analysis, the simplified equation for $f_{scy,0}$, which is consistent in form with that for circular CFST [24, 26, 36], can be obtained:

$$f_{scy,0} = (1.14 + 1.02\xi_s) \cdot f_{ssck} \quad (12)$$

Fig. 19(b) demonstrates the impact of ε_i on $f_{scy,n0}/f_{scy,0}$, where $f_{scy,n0}$ is the axial compressive capacity factor with the initial strain of core concrete considered. Eventually, a linear relationship between $f_{scy,n0}/f_{scy,0}$ and ε_i is obtained according to the regression analysis:

$$f_{scy,n0} = (1.0 + 0.28 \times 10^3 \varepsilon_i) \cdot f_{scy,0} \quad (13)$$

Therefore, the simplified equation for axial capacity (N_u) of circular SSC-FST short columns is as follows:

$$N_u = (1.0 + 0.28 \times 10^3 \varepsilon_i) \cdot f_{scy,0} \cdot A_{sc} \quad (14)$$

The comparison between simplified axial capacities (N_{uc}) using Eq. (14) and numerical/experimental results ($N_{u,fe}$ and N_{ue}) is displayed in Fig. 20. The results show that, the mean value and standard deviation of $N_{uc}/N_{u,fe}$ respectively equal to 1.035 and 0.054, while those of N_{uc}/N_{ue} are 0.929 and 0.112, respectively, indicating that the axial capacity of circular SSC-FST short columns can be accurately predicted using the simplified equations proposed in this study. The application scope of Eq. (14) is: $R=0\sim 100\%$, $\alpha=0.05\sim 0.20$, $f_{cu}=40\text{ MPa}\sim 80\text{ MPa}$, $f_y=235\text{ MPa}\sim 460\text{ MPa}$, and $\varepsilon_i=-300\times 10^{-6}\sim 300\times 10^{-6}$.

5. Conclusions

The axial compressive performance of circular SSC-FST short columns together with the reference circular CFST short columns is experimentally and numerically investigated, and the main conclusions of the present research include:

1 (1) After axial compression tests, the diagonal shear-slip band together with local bulging at both
2 ends of shear-slip band happen to the steel tube regardless of the difference in R and α ; however, a
3 larger α causes a smaller dip angle of the shear-slip band and a slighter local bulging of steel tube.
4 Moreover, crushing/cracking of core concrete appear in the area corresponding to the shear-slip band
5 on steel tube.
6
7
8
9

10 (2) Overall, with the growth of deformation (Δ and ε), the axial load (N) on the specimens goes
11 through three successive stages of development, that is: approximative elastic, elastic-plastic and
12 post-peak. Under the same test parameters, α has a significant effect on the trend of $N - \Delta$ curves,
13 whilst R has no evident impact.
14
15
16
17
18
19
20

21 (3) In general, circular SSC-FST short column specimens have a higher N_{ue} and E_{sc} than their
22 reference counterparts and replacing NFA with fine SSA is more efficacious to enhance the axial
23 capacity of circular SSC-FST short columns when R is the same. Simultaneously, a larger α of the
24 specimens leads to a higher N_{ue} and E_{sc} . On average, $N_{ue}(E_{sc})$ of circular SSC-FST specimens
25 with α of 0.094 and 0.135 are 7.4% (4.6%) and 11.2% (9.2%) higher than their reference counterpart,
26 respectively. Additionally, the composite elastic modulus of circular SSC-FST can be generally
27 calculated based on the superposition principle.
28
29
30
31
32
33
34
35
36
37

38 (4) On the whole, the established FE model can accurately predict the failure patterns, the axial
39 load (axial stress) versus axial shortening (axial strain) relationship and the axial capacity of available
40 composite specimens containing the SSC, by considering the initial strain of core concrete before
41 loading. The simulated results using the FE model exhibit that the composite short columns with a
42 positive ε_i and a larger ξ_s possess a higher p .
43
44
45
46
47
48
49

50 (5) Simplified equations are proposed to predict the axial capacity of circular SSC-FST short
51 columns, and the calculated axial capacities are in good accordance with the numerical and
52 experimental results.
53
54
55
56

57 It is evident that, due to the limited testing capacity and research funds, the size, number and
58 parameter range of the specimens in this paper cannot cover all the circular SSC-FST columns in
59
60
61
62
63
64
65

practical engineering. As a result, more tests of such composite columns are needed to guide the practical design and further verify the FE model.

Declaration of Competing Interest:

The authors declare that they have no known competing financial interests or personal relationships that could have appeared to influence the work reported in this paper.

Acknowledgements:

The studies in this paper are financially supported by the National Natural Science Foundation of China (Grant No. 51678105). The financial support is gratefully acknowledged. The authors also wish to thank Mr. Xu-Liang Sun for his assistance in the experiments.

References:

- [1] Baalamurugan J, Ganesh Kumar V, Chandrasekaran S, Balasundar S, Venkatraman B, Padmapriya R, Bupesh Raja VK. Recycling of steel slag aggregates for the development of high density concrete: Alternative & environment-friendly radiation shielding composite. *Compos Part B: Eng* 2021;216:108885.
- [2] Pang B, Zhou Z, Xu H. Utilization of carbonated and granulated steel slag aggregate in concrete. *Constr and Build Mater* 2015;84:454-67.
- [3] Piro SN, Mohammed AS, Hamad SM. Compressive strength and piezoresistivity of smart cement paste modified with waste steel slag. *J of Build Eng* 2023;70:106393.
- [4] Pellegrino C, Cavagnis P, Faleschini F, Brunelli K. Properties of concretes with black/oxidizing electric arc furnace slag aggregate. *Cem and Concr Compos* 2013;37:232-40.
- [5] Abendeh RM, Salmana D, Louzi RA. Experimental and numerical investigations of interfacial bond in self-compacting concrete-filled steel tubes made with waste steel slag aggregates. *Dev in the Built Environ* 2022;11:100080.
- [6] Sharba AA. The efficiency of steel slag and recycled concrete aggregate on the strength properties of concrete. *KSCE J of Civ Eng* 2019;23(11):4846-51.
- [7] Wen X, Zhou J, Chen B, Deng Z, Liu B. Mechanical performance of steel slag concrete under biaxial compression. *Mater* 2020;13(15):3268.
- [8] Brand AS, Roesler JR. Steel furnace slag aggregate expansion and hardened concrete properties. *Cem and Concr Compos* 2015;60:1-9.
- [9] Guo J, Bao Y, Wang M. Steel slag in China: Treatment, recycling, and management. *Waste Manag* 2018;78:318-30.

- 1
2
3
4
5
6
7
8
9
10
11
12
13
14
15
16
17
18
19
20
21
22
23
24
25
26
27
28
29
30
31
32
33
34
35
36
37
38
39
40
41
42
43
44
45
46
47
48
49
50
51
52
53
54
55
56
57
58
59
60
61
62
63
64
65
- [10] Qasrawi H, Shalabi F, Asi I. Use of low CaO unprocessed steel slag in concrete as fine aggregate. *Constr and Build Mater* 2009;23(2):1118-25.
- [11] Warudkar A, Elavenil S. Strength and durability properties of waste steel slag mixed concrete. *Eng rev* 2020;42(1):1628.
- [12] Yu X. Concrete made with steel slag and waste glass and its application in concrete-filled steel tubular columns. Australia, Western Sydney University, 2017.
- [13] Papayianni I, Anastasiou E. Production of high-strength concrete using high volume of industrial by-products. *Constr and Build Mater* 2010;24(8):1412-7.
- [14] Zou J, Jin Z, Chen D, Gao H. Experimental study on volume deformation of iron tailing-steel slag aggregate concrete. *IOP Conf Ser Earth and Environ Sci* 2019;242(5):052061.
- [15] Yu X, Tao Z, Song TY, Pan Z. Performance of concrete made with steel slag and waste glass. *Constr and Build Mater* 2016;114:737-46.
- [16] Han LH, Li W, Bjorhovde R. Developments and advanced applications of concrete-filled steel tubular (CFST) structures: Members. *J of Constr Steel Res* 2014;100:211-28.
- [17] Yu F, Fang Y, Zhang Y, Xu L, Bai R. Mechanical behavior of self-stressing steel slag aggregate concrete filled steel tubular short columns. *Struct Concr* 2020;21(4):1597-611.
- [18] Yu X, Tao Z, Song TY. Effect of different types of aggregates on the performance of concrete-filled steel tubular short columns. *Mater and Struct* 2016;49:3591-605.
- [19] Yang YF, Fu F, Zhang YQ. Static performance of steel slag concrete filled steel square hollow section members. *J of Constr Steel Res* 2023;205:107896.
- [20] Lai MH, Lin YH, Jin YY, Fei Q, Wang ZC, Ho JCM. Uni-axial behaviour of steel slag concrete-filled-steel-tube columns with external confinement. *Thin-Walled Struct* 2023;185:110562.
- [21] Luo C, Wang F, Chen H, Qi A, Chen Y. Study on the hysteretic behavior of recycled aggregate concrete-filled steel tube columns containing ferronickel slag. *J Build Eng* 2022;46:103695.
- [22] Yang YF, Hou C, Liu M. Tests and numerical simulation of rectangular RACFST short columns under concentric compression. *Struct* 2020;27:396-410.
- [23] Hou C, Han LH, Zhao XL. Concrete-filled circular steel tubes subjected to local bearing force: Experiments. *J of Constr Steel Res* 2013;83:90-104.
- [24] Han LH. Concrete filled steel tubular structures-theory and practice (3rd Edition), Beijing, China: Science Press; 2016. (in Chinese).
- [25] ABAQUS. Simulia 6.14 analysis user's manual, Providence, RI, USA: Dassault Systemes Simulia Corp; 2014.
- [26] Zhao XL, Han LH, Lu H. Concrete-filled tubular members and connections. Oxford, UK: Taylor and Francis; 2010.

[27]ACI Committee 209. Prediction of creep, shrinkage, and temperature effects in concrete structures (ACI 209R-92), Farmington hills, MI, USA: American Concrete Institute; 1992.

[28]Yang YF, Fu F, Bie XM, Dai XH. Axial compressive behaviour of CFDST short columns with large void ratio. J of Constr Steel Res 2021;186:106892.

[29]GB/T 51446. Technical standard for concrete-filled steel tubular hybrid structures. Beijing: China Architecture & Building Press; 2021.

[30]Comité Euro-International du Béton. CEB-FIP model code 1990, London, UK: Thomas Telford Services; 1993.

[31]ACI Committee 318. Building code requirements for structural concrete (ACI 318-19) and commentary, Farmington hills, MI, USA: American Concrete Institute; 2019.

[32]Birtel V, Mark P. Parameterised finite element modelling of RC beam shear failure. Proceedings of the 19th Annual International ABAQUS Users' Conference, Boston, USA, 2006, pp. 95-108.

[33]CEN. EN 1992-1-1, Eurocode 2: Design of concrete structures-Part 1-1: General rules and rules for buildings, Brussels, Belgium: European Committee for Standardization; 2004.

[34]Lyu WQ, Han LH, Hou Chao. Axial compressive behaviour and design calculations on recycled aggregate concrete-filled steel tubular (RAC-FST) short columns. Eng Struct 2021;241:112452.

[35]Zhang X, Zhang S, Fan Y, Ding Y, Wang X, Meng E. The axial compressive behavior of stone-lightweight aggregate concrete-filled steel tubular short columns. Constr and Build Mater 2021;298:123815.

[36]Abadel AA, Khan MI, Masmoudi R. Experimental and numerical study of compressive behavior of axially loaded circular ultra-high-performance concrete-filled tube columns. Case Stud in Constr Mater 2022;17:e01376.

Replies to Reviewer's Comments

Structures

Manuscript: Performance of SSC filled circular steel tube short columns under axial compression
(Ms. Ref. No.: STRUCTURES-D-23-02843)

Authors: Shi-Qi Zhou, You-Fu Yang*, Feng Fu
(* Corresponding author: youfuyang@163.com)

The authors wish to thank the reviewers' comments which certainly enhance the quality of the paper.

The authors have checked all the editorial revisions and the comments from the reviewers and revised the manuscripts accordingly. The changes we have made in response to the reviewers' comments are listed in the following tables.

Reviewer #2

No.	Comments, replies and changes made.	
General	Comment	The paper presents experimental and numerical investigation on performance of steel slag concrete filled circular steel tube short columns under axial compression. A group of tests was carried out, A FE model was developed and validated against test results, acceptable agreement reached. A simple formula developed to assess the axial capacity of this type of short composite columns. The subject matter is interesting and content is original. The research provides useful information to the use of steel slag for structural concrete and column member. The following clarification/improvement/correction is suggested.
	Replies	The authors would like to thank for the reviewer's comments. Your comments have helped us to improve the quality of our paper, which can be found from the detailed changes summarized as follows.
1	Comment	Overall the paper, letter "E" is mostly used for material elastic modulus, such as E_c , E_s , E_{sc} ... etc. however, " E_i " is used for strain. Why not use another character/letter for this strain?
	Replies	The authors agree with the reviewer's comments that " E_i " for strain is not professional. A new variable has been used for the initial strain of core concrete before loading.
	Changes made	For the whole paper, including text, tables and figures, " E_i " is replaced by ε_i to ensure the unity of the meaning of variables.
2	Comment	Page 13, lines 40-43: it would be better to change "1.0E-6" to "10-6" (exponential form). Is there any specific meaning for the format of "2.36E-5"? If not, why not simplify it and use a general numerical value?
	Replies	The authors agree with the reviewer's comments. Moreover, there is no specific meaning for the format of "2.36E-5"; however, to ensure as much consistency as possible after the decimal point of the significant number, the scientific notation is used because "2.36E-5" is a relatively small number.
	Changes made	The related content has been changed to the following format: $\varepsilon_{c,u} = (1300 + 12.5f'_{SSC} + 800\xi_s^{0.2}) \times 10^{-6}$ <p>To ensure consistency of expression, the related content has been changed to the following format:</p> $\beta_0 = 1.25\sqrt{f'_{SSC}} \times (2.36 \times 10^{-5})^{[0.25+(\xi_s-0.5)^7]} \geq 0.12$

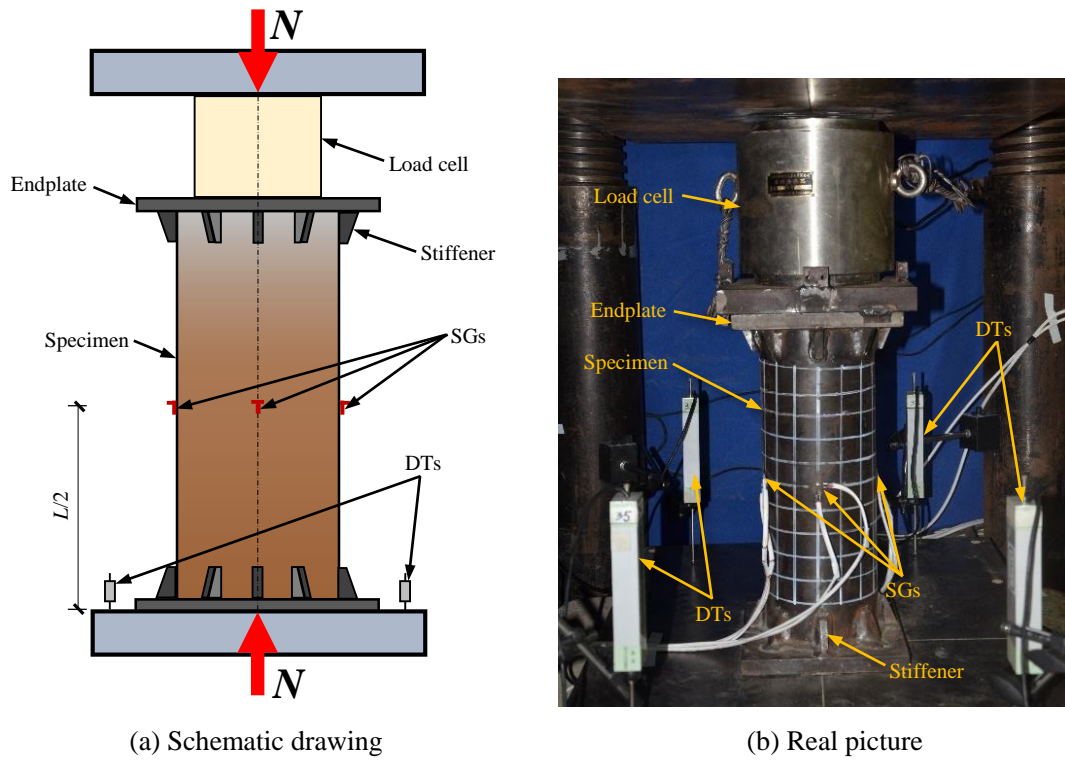
3	Comment	Page 17, formula (11): it would be better to change "1.0E-6" to "10 ⁻⁶ "(exponential form)
	Replies	The authors agree with the reviewer's comments.
	Changes made	The formula has been changed to the following format: $\epsilon_{a,y} = [1300 + 12.5f'_{SSC} + (600 + 33.3f'_{SSC}) \cdot \xi_s^{0.2}] \times 10^{-6} \quad (11)$
4	Comment	There are so many parameters/variables in this paper, it is suggested to have a list for the symbol definitions at the beginning or end.
	Replies	The authors agree with the reviewer's comments.
	Changes made	A list of the symbol definitions with the title of 'Nomenclature' has been added to the beginning of the revised manuscript.
5	Comment	Discuss/clarify the application range and limitation of your research results/conclusions due to limitation of specimen number and dimension etc.
	Replies	The authors agree with the reviewer's comments.
	Changes made	The following contents have been added to the end of the revised manuscript to discuss/clarify the application range and limitation of our research results/conclusions. It is evident that, due to the limited testing capacity and research funds, the size, number and parameter range of the specimens in this paper cannot cover all the circular SSC-FST columns in practical engineering. As a result, more tests of such composite columns are needed to guide the practical design and further verify the FE model.

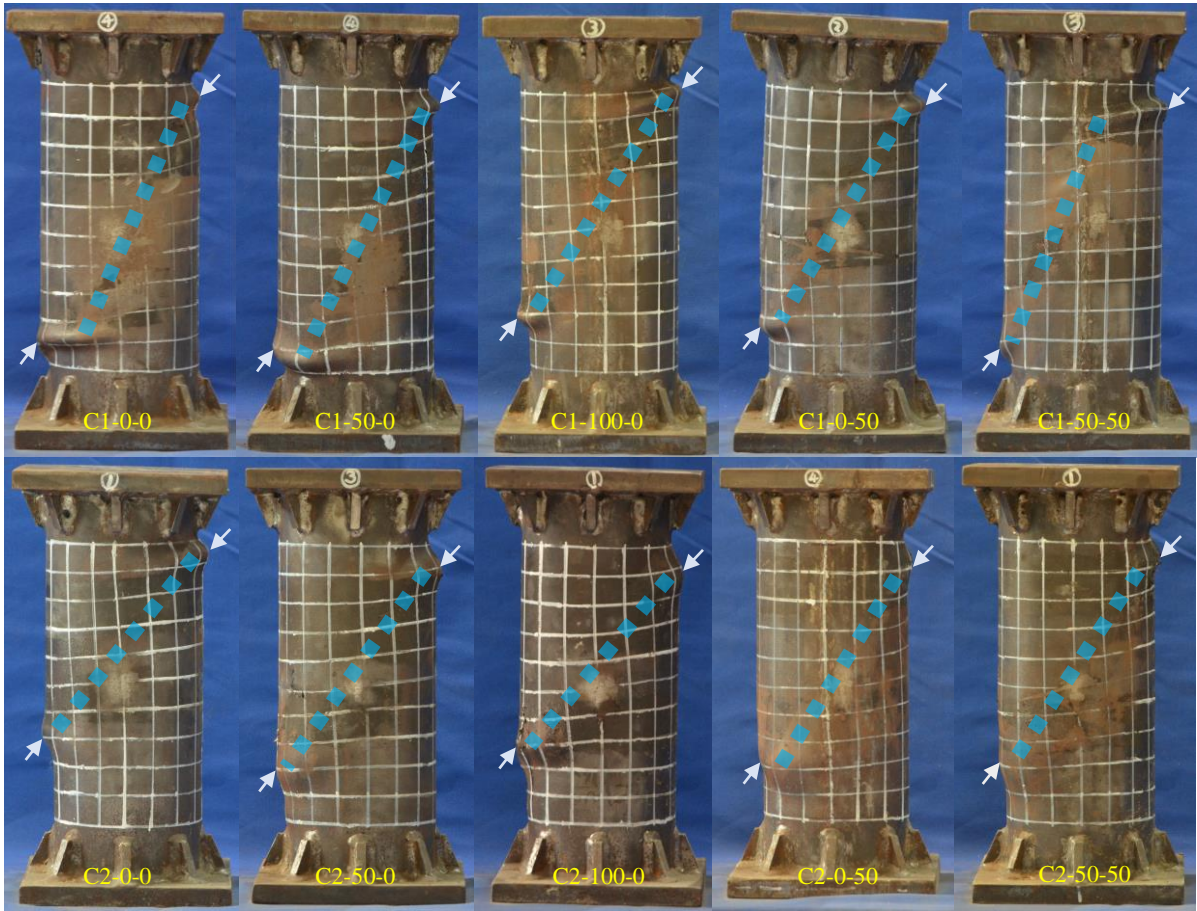
Reviewer #3

No.	Comments, replies and changes made.	
General	Comment	This paper presents an experimental and numerical study on the performance of steel slag concrete (SSC) filled circular steel tube columns under axial compression. The topic is new and interesting, proposing an innovative alternative for reusing industrial waste. The tests are carefully conducted and introduced, with a numerical model established. Simplified design method is also proposed to provide a reference for practice. The manuscript is well written and organized. Publication is recommended once the following comments are addressed.
	Replies	The authors really appreciate the reviewer's commendation and comments. Your comments have helped us to improve the quality of this paper, which can be seen from the detailed changes summarized in this report.
1	Comment	Page 4, Lines 53-56. The shape of the end plates mentioned in the article are circular, however, the end plates at both ends of the specimens are square in Figs. 1, 2 and 3. Please clarify. Plus, please provide the dimensions of the stiffeners in the text as well.
	Replies	We are sorry for the confusion caused by us. The related contents have been revised in the manuscript.
	Changes made	The third paragraph of Section 2.1: 'Before casting the concrete, one square steel plate with 210 mm side length and 15 mm thickness was welded to ... another square steel plate same as ...eight pairs of right-angle trapezoidal stiffeners with 10 mm thickness spaced equally ...'

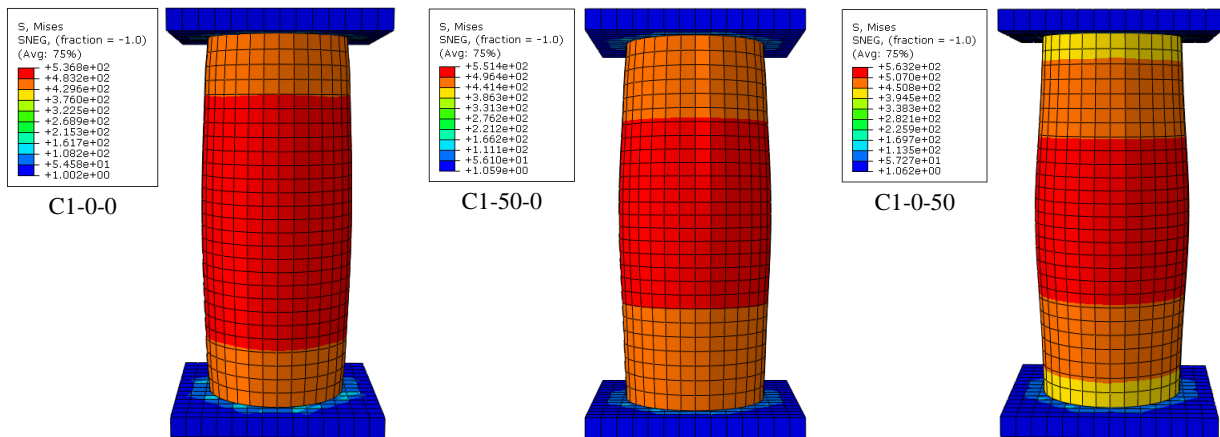
2	Comment	Page 12, Lines 4-7. Please clearly state which parameters will affect the correction factor in formula (5), and whether they have all been taken into account in the current calculation process.
	Replies	The authors agree with the reviewer's comments. The related contents have been revised in the manuscript.
	Changes made	The paragraph following Eq. (6): '... mix proportion, that is, loading age, fine aggregate percentage, cement content and air content are the same.'
3	Comment	Page 14, Lines 8-11. What is the basis for using cracking criterion to simulate the tensile property of core SSC in the plastic stage. Please briefly comment. Plus, would the interface bonding between the SSC and the steel tube affect the compressive behaviour much? Some discussions on the influence of steel-concrete bonding in resisting axial and local bearing in JCSR, 83: 90-104 might be helpful.
	Replies	We are very sorry for the confusion caused by us. The concrete tension stiffening can be simulated by means of a post-failure stress-strain relationship or by applying a fracture energy-based approach. However, when there is no reinforcement in significant regions of the model, the first approach may introduce unreasonable mesh sensitivity, whilst the fracture energy based approach can give a more stable result. Moreover, the authors agree with the reviewer's comments that interface bonding needs to be discussed. The related contents have been revised in the manuscript.
	Changes made	The paragraph following Eq. (10): 'According to the achievement in [19], the tensile property ...' The following contents have been added to the end of the first paragraph of Section 2.4: 'It should be noted that the bonding between SSC and steel tube might be critical for the axial and lateral compression behaviour of the composite columns [23], which needs further investigation.' Accordingly, a new reference has been added to the revised manuscript: [23] Hou C, Han LH, Zhao XL. Concrete-filled circular steel tubes subjected to local bearing force: Experiments. J of Constr Steel Res 2013;83:90-104.
4	Comment	The formula given in Fig. 19 is inconsistent with equation (13) and (14) in the text. Please double check.
	Replies	We are sorry for the confusion caused by us. There were clerical errors in our writing. The related contents have been revised in the manuscript.
	Changes made	The formulae have been changed to the following format: $f_{scy,n0} = (1.0 + 0.28 \times 10^3 \varepsilon_i) \cdot f_{scy,0} \quad (13)$ $N_u = (1.0 + 0.28 \times 10^3 \varepsilon_i) \cdot f_{scy,0} \cdot A_{sc} \quad (14)$
5	Comment	For equation (12), the new national standard DB/T 51446 is recommended to be referred to.
	Replies	The authors agree with the reviewer's comments. The related contents have been revised in the manuscript.
	Changes made	The sentence before Eq. (12): '... in form with that for circular CFST [24, 26, 36], can be ...' Accordingly, a new reference has been added to the revised manuscript:

		[36] GB/T 51446. Technical standard for concrete-filled steel tubular hybrid structures. Beijing: China Architecture & Building Press; 2021.
6	Comment	In Fig. 12, the two figures are suggested to be with a similar size for better display.
	Replies	The authors agree with the reviewer's comments.
	Changes made	Two figures in Fig. 12 have been revised to have a similar size.

Figures:**Fig. 1.** Test set-up.

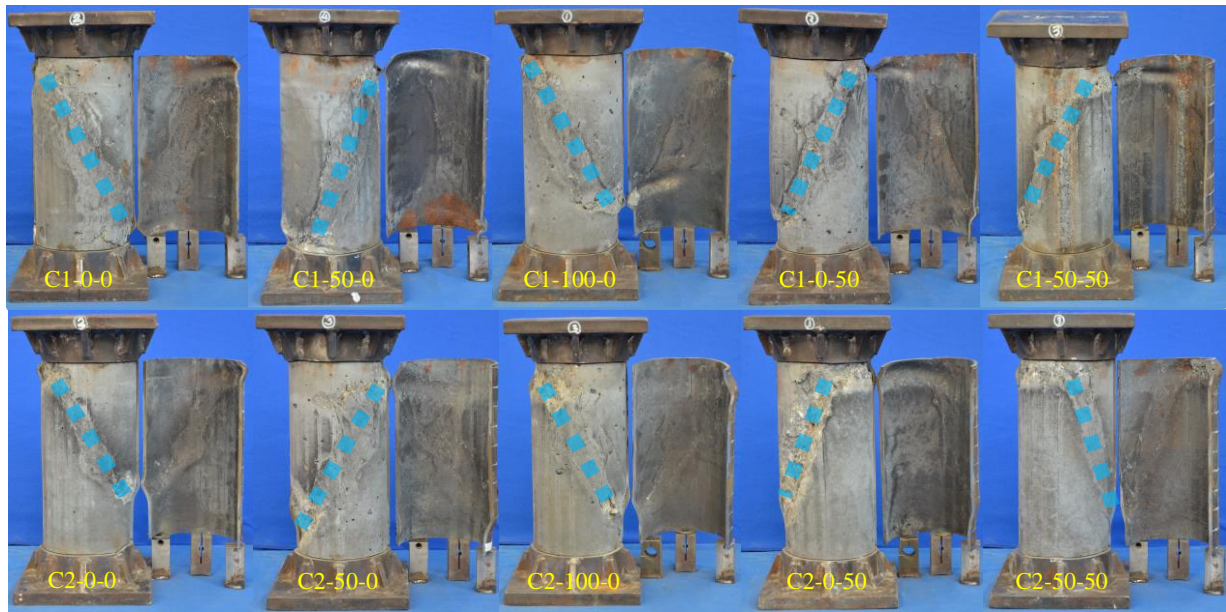


(a) Test results

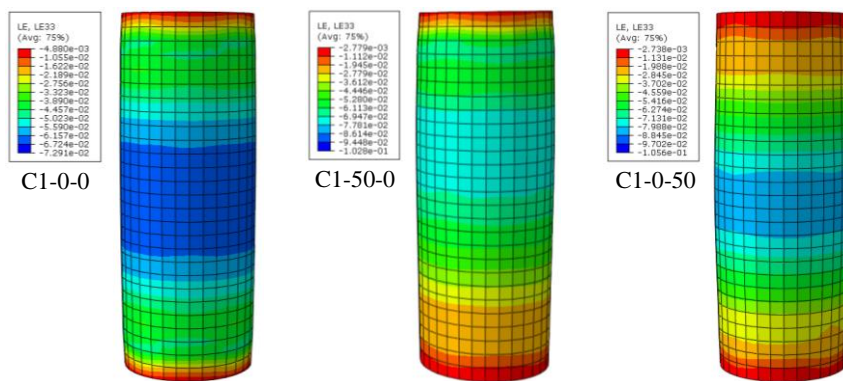


(b) Typical simulation results

Fig. 2. Failure pattern of the specimens.



(a) Test results



(b) Typical simulation results

Fig. 3. Failure pattern of core concrete.

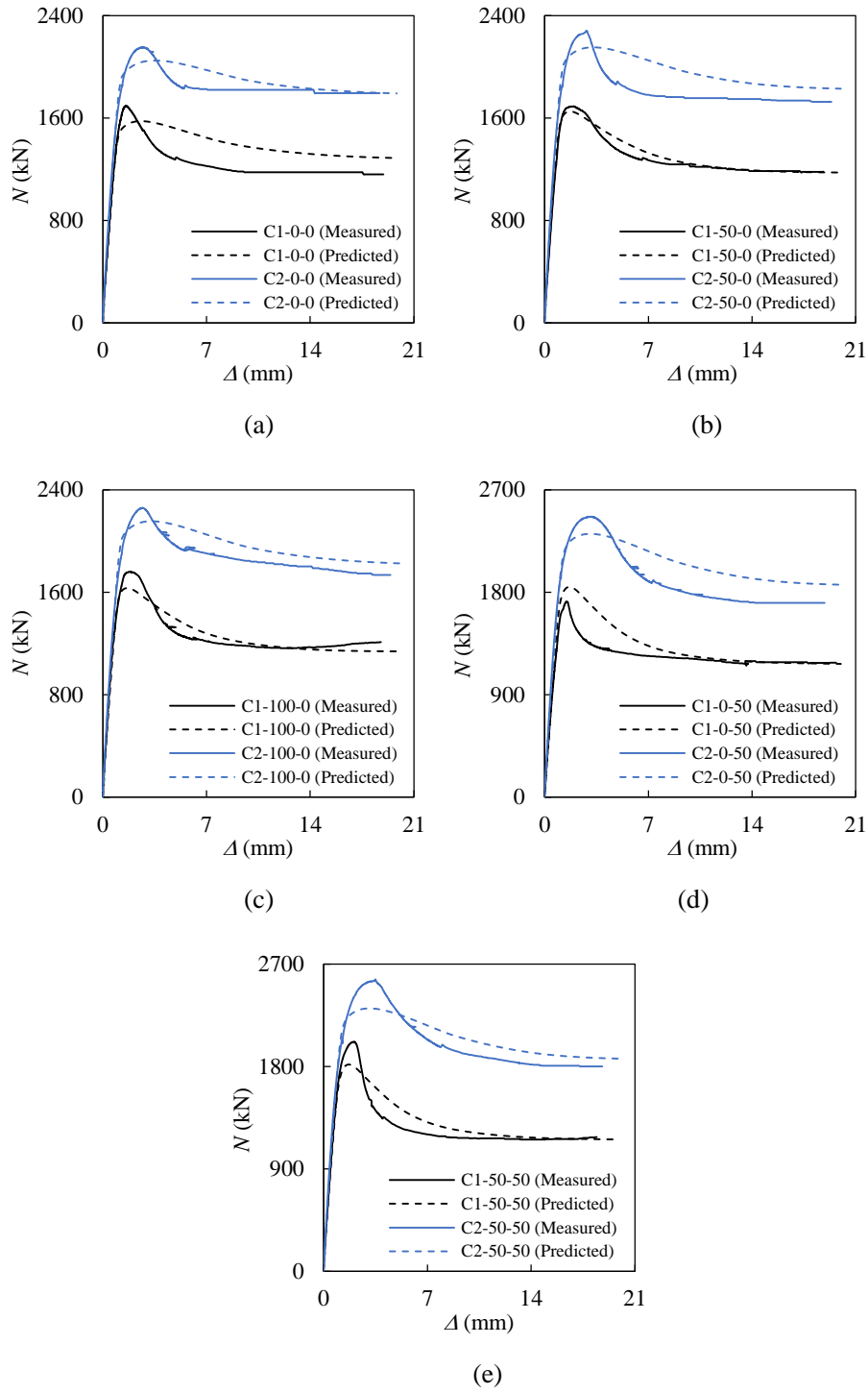
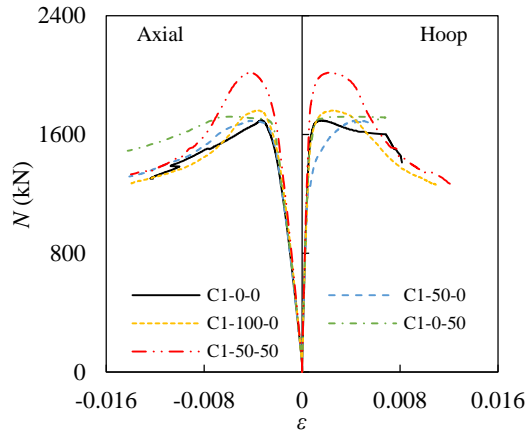
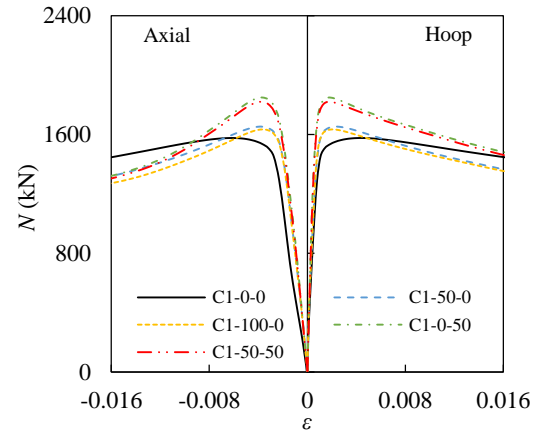


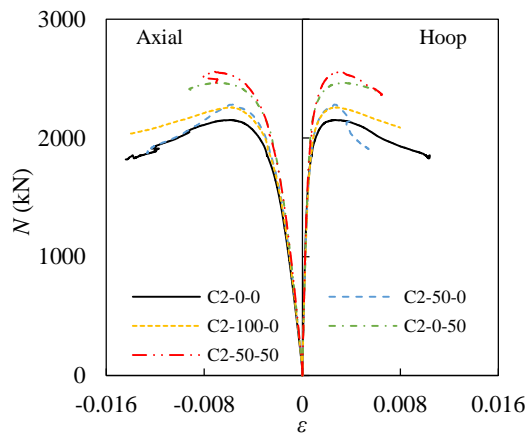
Fig. 4. Axial load (N) versus axial shortening (Δ) curves of the specimens.



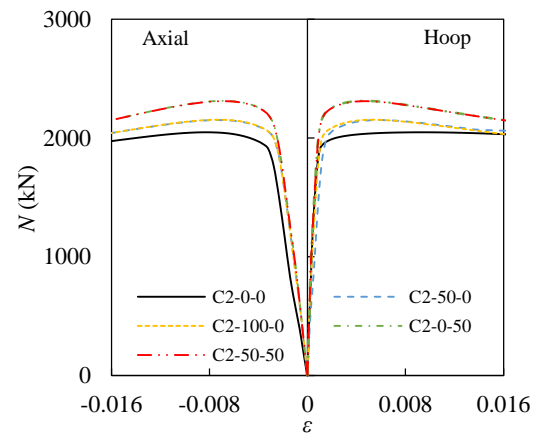
(a-1) C1 series (measured)



(a-2) C1 series (predicted)



(b-1) C2 series (measured)



(b-2) C2 series (predicted)

Fig. 5. Axial load (N) versus strain (ϵ) curves of the specimens.

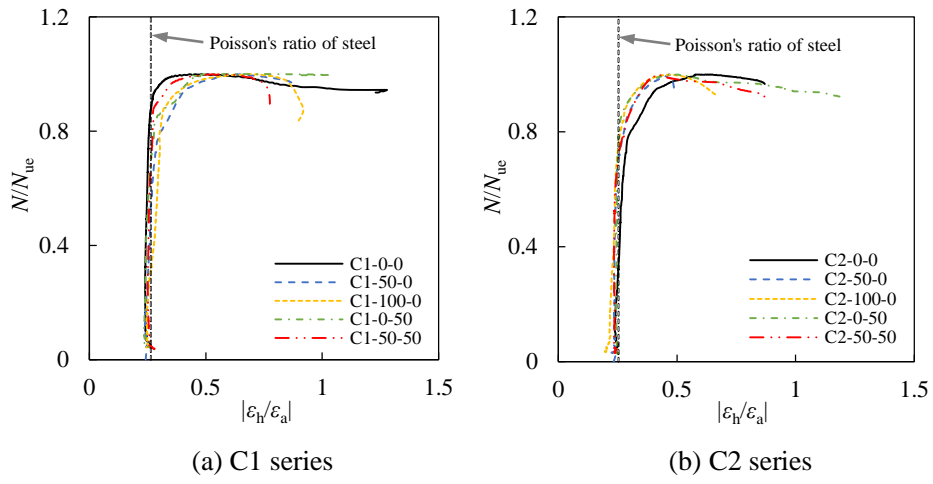


Fig. 6. N/N_{ue} versus $|\epsilon_h/\epsilon_a|$ relationship of the specimens.

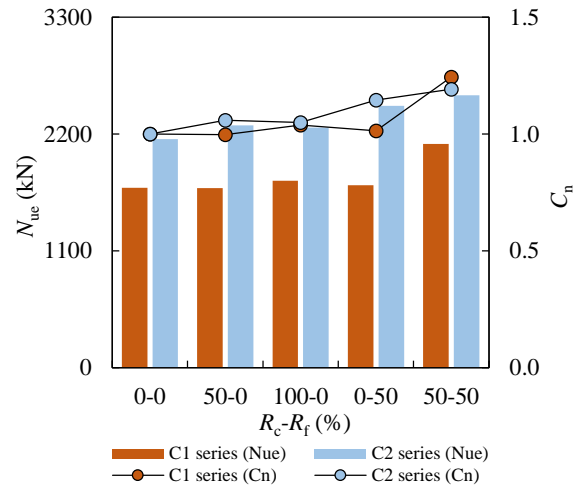


Fig. 7. Effect of parameters on N_{ue} and C_n of the specimens.

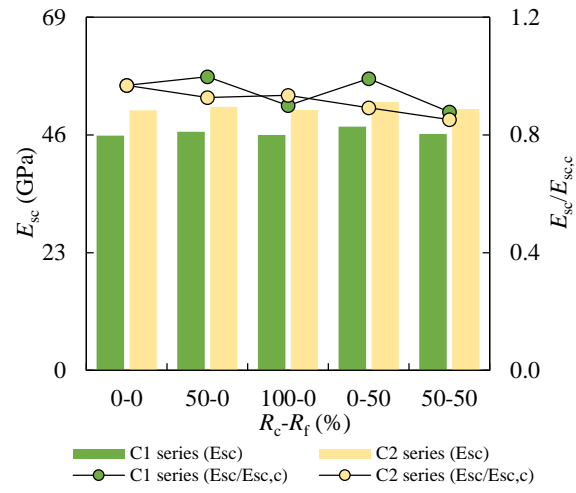


Fig. 8. Variation of E_{sc} and $E_{sc}/E_{sc,c}$ of the specimens.

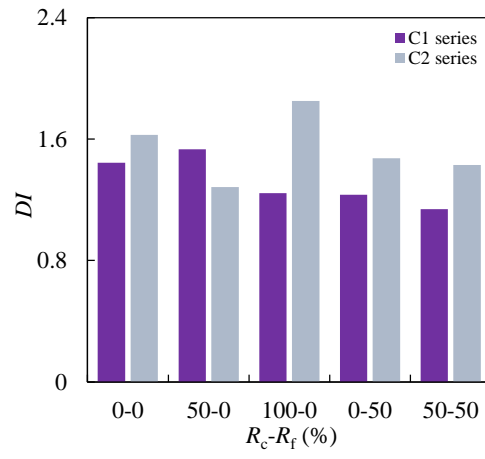


Fig. 9. Ductility index (DI) of the specimens.

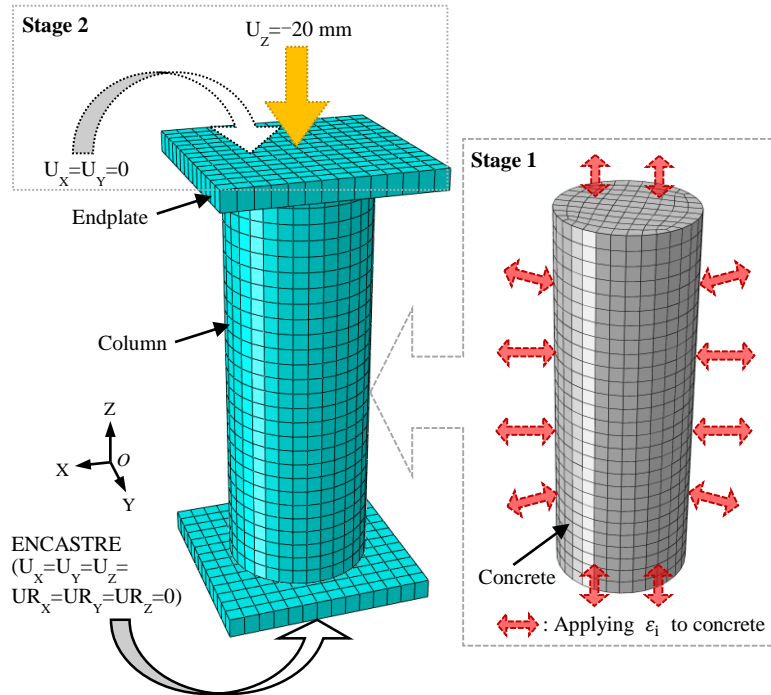
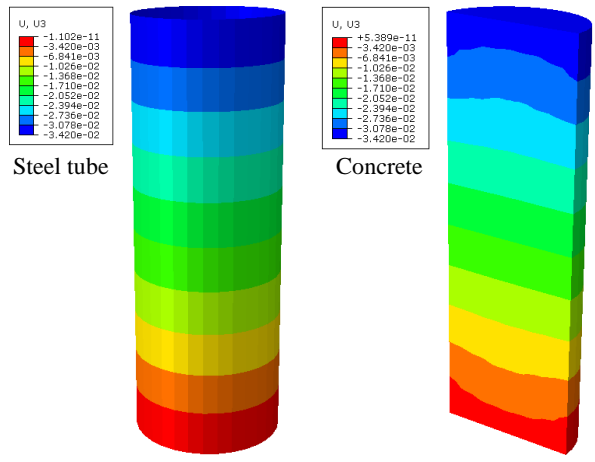
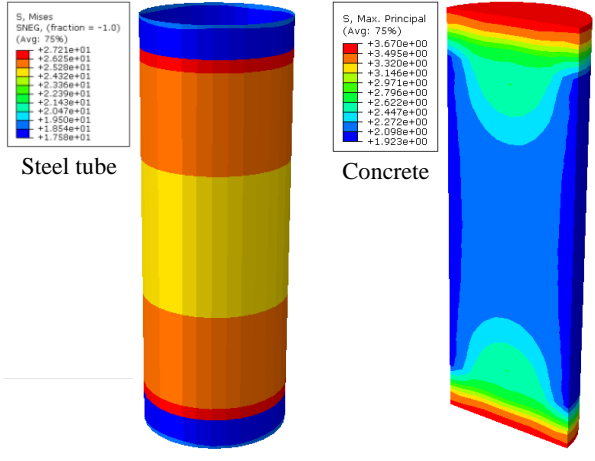


Fig. 10. Meshing and boundary conditions for the FE model of axially compressed circular SSC-FST short columns.

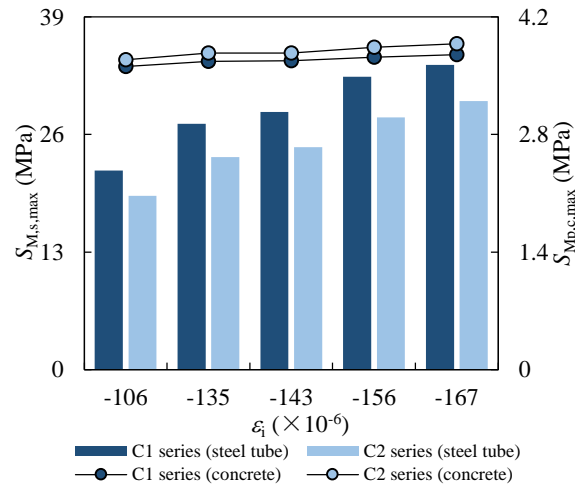


(a) Displacement

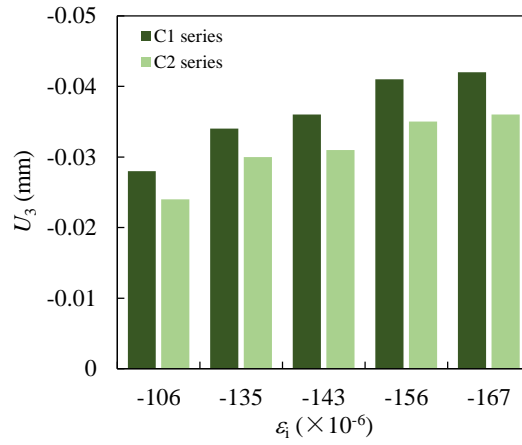


(b) Stress

Fig. 11. The predicted field variables of specimen C1-50-50 before loading.

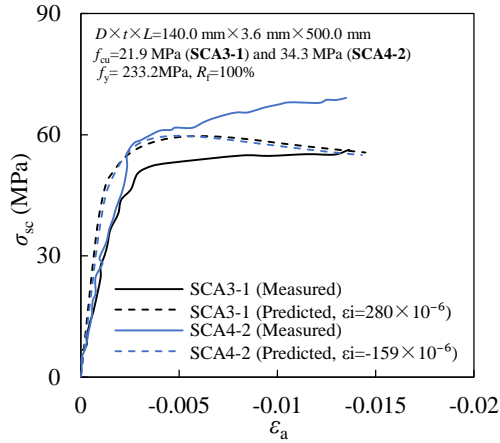


(a) Maximum stress ($S_{M,s}$, $S_{Mp,c}$)

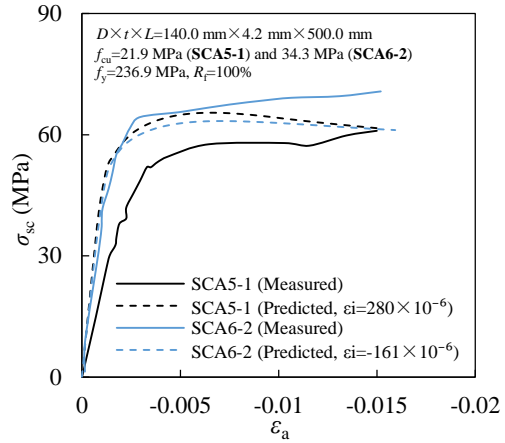


(b) Displacement

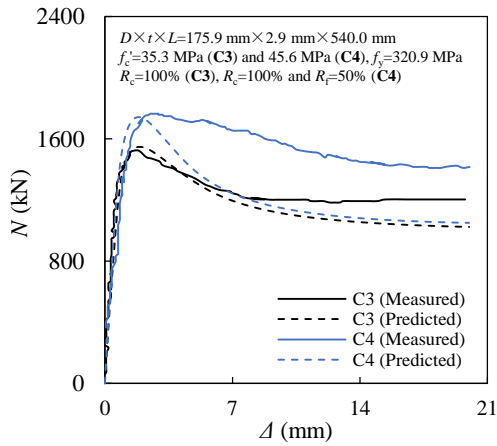
Fig. 12. Effect of ϵ_i on typical field variables of all the specimens.



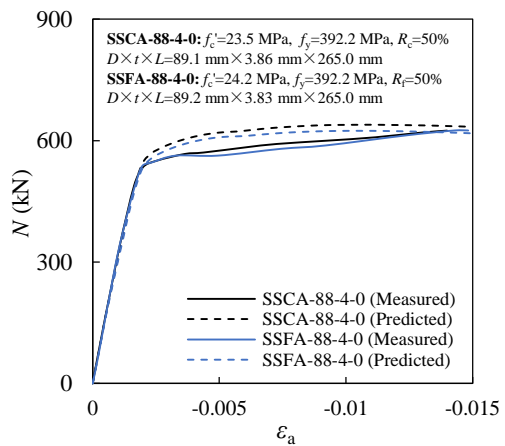
(a) Tests of Yu et al. [17]



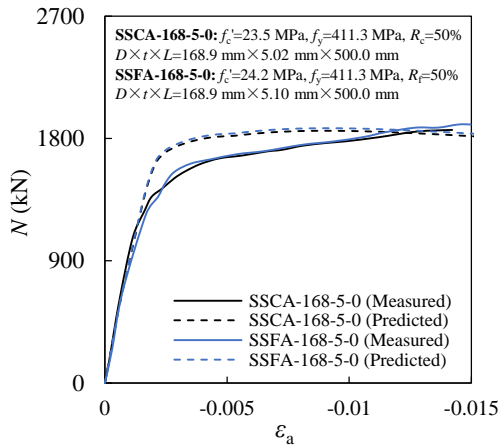
(b) Tests of Yu et al. [17]



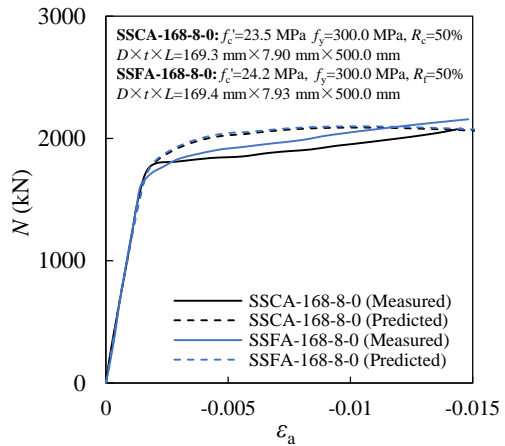
(c) Tests of Yu et al. [18]



(d) Tests of Lai et al. [20]



(e) Tests of Lai et al. [20]



(f) Tests of Lai et al. [20]

Fig. 13. Representative contrast between the predicted and measured axial load (axial stress) versus axial shortening (axial strain) curves in the literature.

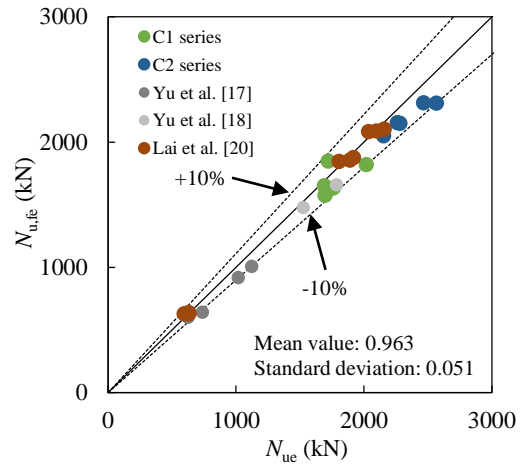


Fig. 14. Comparison between $N_{u,fe}$ and N_{ue} of circular SSC-FST short column specimens.

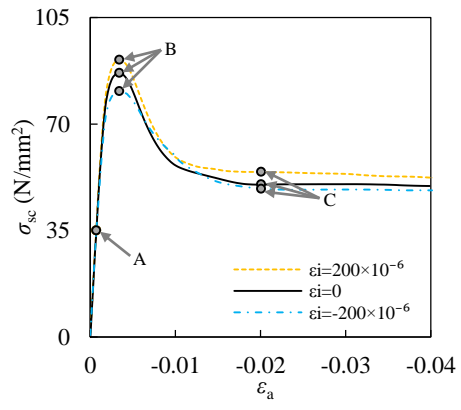


Fig. 15. The simulated σ_{sc} - ϵ_a curve of typical circular SSC-FST short columns.

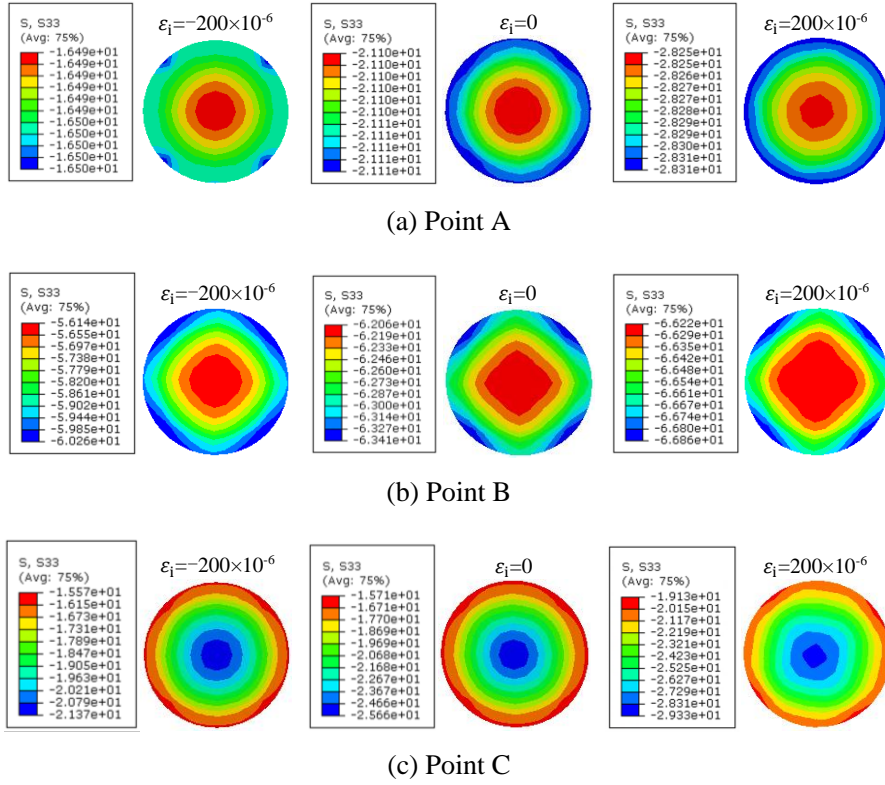


Fig. 16. Stress field of core SSC at the mid-height section of typical circular SSC-FST short columns.

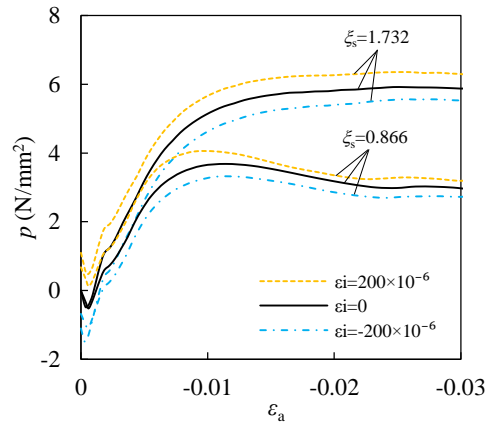


Fig. 17. Effect of ϵ_i and ξ_s on the interaction stress (p) between steel tube and core concrete.

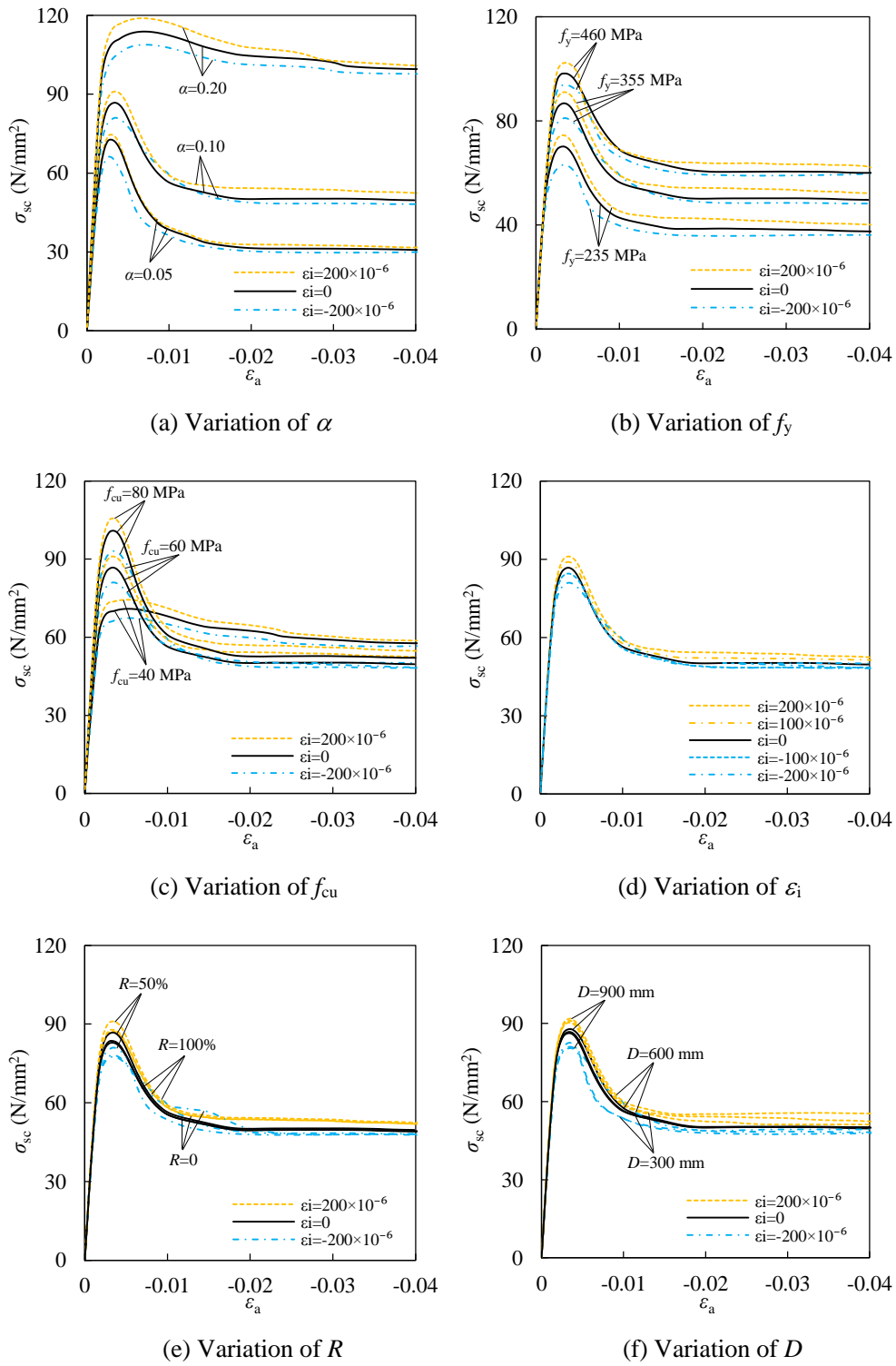
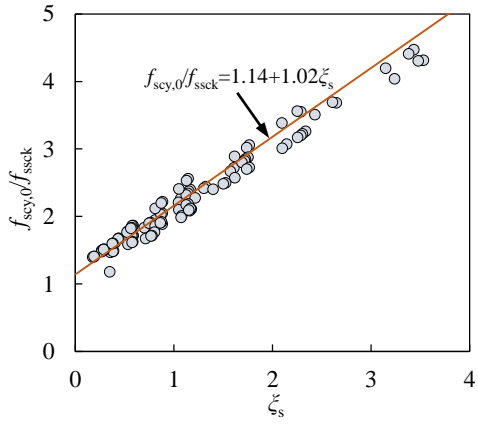
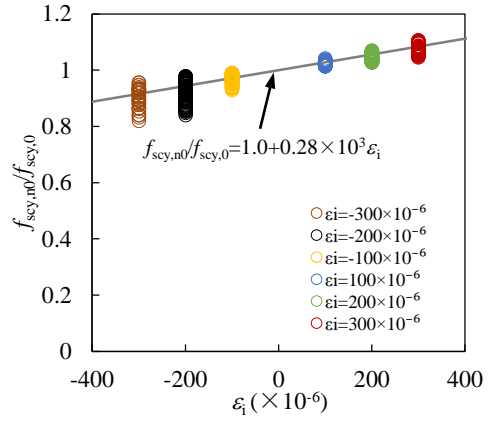


Fig. 18. Effect of typical parameters on σ_{sc} - ϵ_a curve of circular SSC-FST short columns.

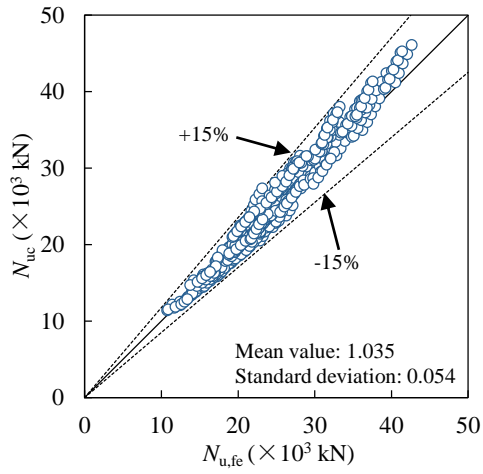


(a) $f_{scy,0}/f_{ssck}$ - ξ_s relationship

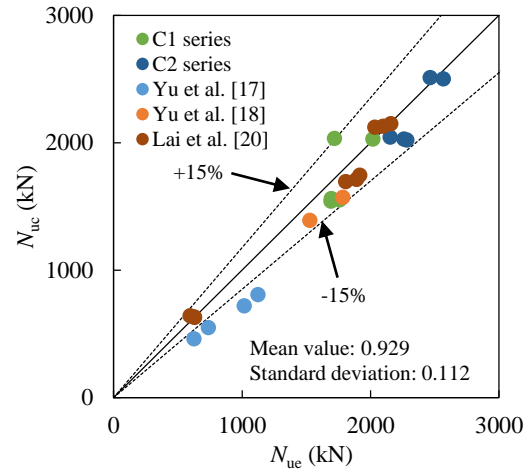


(b) $f_{scy,n0}/f_{scy,0}$ - ϵ_i relationship

Fig. 19. Strength index (f_{scy}) of circular SSC-FST short columns.



(a) N_{uc} and $N_{u,fe}$



(b) N_{uc} and N_{ue}

Fig. 20. Comparison between simplified axial capacities and numerical/experimental results.

Tables:**Table 1.** Information of the specimens.

No.	Label	D (mm)	t (mm)	L (mm)	α	R_c (%)	R_f (%)	f_y (MPa)	f_{cu} (MPa)	E_{sc} (GPa)	N_{ue} (kN)	$N_{u,fe}$ (kN)	$N_{u,fe}/N_{ue}$
1	C1-0-0	150.0	3.33	450.0	0.094	0	0	449.7	51.2	47.4	1695.3	1575.6	0.929
2	C1-50-0	150.0	3.33	450.0	0.094	50	0	449.7	61.1	46.7	1691.2	1651.0	0.976
3	C1-100-0	150.0	3.33	450.0	0.094	100	0	449.7	61.9	51.1	1760.0	1633.9	0.928
4	C1-0-50	150.0	3.33	450.0	0.094	0	50	449.7	76.8	48.1	1719.0	1848.6	1.075
5	C1-50-50	150.0	3.33	450.0	0.094	50	50	449.7	76.8	52.5	2018.0	1819.3	0.902
6	C2-0-0	150.0	4.59	450.0	0.135	0	0	518.5	51.2	52.4	2153.2	2049.0	0.952
7	C2-50-0	150.0	4.59	450.0	0.135	50	0	518.5	61.1	55.6	2281.4	2151.2	0.943
8	C2-100-0	150.0	4.59	450.0	0.135	100	0	518.5	61.9	54.5	2260.0	2154.1	0.953
9	C2-0-50	150.0	4.59	450.0	0.135	0	50	518.5	76.8	58.8	2465.0	2313.9	0.939
10	C2-50-50	150.0	4.59	450.0	0.135	50	50	518.5	76.8	59.9	2566.1	2310.7	0.900

Table 2. Properties of different aggregates.

Type	Apparent gravity (kg/m ³)	Bulk density (kg/m ³)	Absorption rate (%)	Crushing index (%)	Fineness modulus
Coarse SSA	3472	1806	1.65	5.7	-
NCA	2718	1443	1.10	11.9	-
Fine SSA	2629	1440	2.5	-	2.34
NFA	3189	1926	5.0	-	2.98

Table 3. Mix proportions and properties of concrete.

Label [#]	Mix proportions (kg/m ³)								Properties						
	Cement	Water	NCA	Coarse SSA	NFA	Fine SSA	Fly ash	Superplasticizer	E_c (GPa)	f_{cu28} (MPa)	f_{cu} (MPa)	Slump (mm)	Spread (mm)	IS ($\times 10^{-6}$)	ϵ_i ($\times 10^{-6}$)
0-0	398	200	770	0	795	0	170	5	32.4	46.3	51.2	270	645	-404	-167
50-0	398	200	385	385	795	0	170	5	33.2	57.7	61.1	280	660	-378	-156
100-0	398	200	0	770	795	0	170	5	32.5	53.3	61.9	265	675	-346	-143
0-50	398	200	770	0	398	398	170	5	34.3	64.3	76.8	260	710	-258	-107
50-50	398	200	385	385	398	398	170	5	32.7	69.7	76.8	265	690	-326	-135

Note: [#], the first and second numbers represent numerator of R_c and R_f , respectively.